DEVELOPMENT OF A NOVEL TIME-OF-FLIGHT LASER RANGEFINDER FOR OPTO-MECHATRONIC APPLICATIONS

by

© Michael Morgan

A Thesis submitted to the

School of Graduate Studies

in partial fulfillment of the requirements for the degree of

Masters of Engineering

Engineering and Applied Science

Memorial University of Newfoundland

May 2020

St. John's Newfoundland and Labrador

ABSTRACT

A Laser rangefinder is an opto-electric device used to determine the distance between two objects. There are many applications for laser rangefinders in industries such as unmanned vehicles, defence sectors, scientific exploration, and outdoor sporting activities. In this work a novel time-of-flight laser rangefinder was designed to deliver range information while meeting size weight and power constraints. The laser rangefinder consists of three main systems, optical, electrical, and mechanical. The optical system consists of collimating transmitting optics and a focusing mirror for receiving optics. The electrical system is comprised of a pulsing circuit providing a narrow pulse with high peak current, a receiving circuit for identifying the return signal, and an FPGA controller for triggering the pulse and calculating distance. The mechanical system is made up of the housing of the laser rangefinder which ensures concentricity and spacing of the optical system.

ACKNOWLEDGEMENTS

I would like to thank Dr. Nichols Krouglicof for his guidance and support throughout the research and writing process, ACOA, Boeing, and RDC for funding the INSPIRUS Project which allowed this research to be possible, the staff of the Mechantronics Development and Prototyping Facility at Memorial University, and all others at Memorial University who provided aid through this project.

Table of Contents

List of Figures

List of Tables

List of Appendices

List of Abbreviations and Acronyms

ASIC	Application Specific Integrated Circuit
CAD	Computer Aided Design
EFL	Effective Focal Length
FPGA	Field Programmable Gate Array
GaAs	Gallium Arsenide
IOR	Index of Refraction
MSE	Mean Square Error
Nd:YAG	Neodymium-doped Yttrium Aluminum Garnet
Op-Amp	Operational Amplifier
PIN	Positive-Intrinsic-Negative
PKM	Parallel Kinematic Mechanism
PLL	Phase Locked Loop
RC	Resistor-Capacitor
RF	Radio Frequency
SWaP	Size Weight and Power

Chapter 1: Introduction

1.1. Project Background

The Intelligent Sensor Platforms for Unmanned Vehicles project under the supervision of Dr. Nicholas Krouglicof began at Memorial University in 2010. This project was the response to a proposal for the development of an opto-electric method of sense and avoid for unmanned vehicles. Due to changing regulations on the use of unmanned aerial vehicles in commercial air space there is an increasing demand for a reliable system that can be used to detect airborne objects, such as commercial aircraft, and move out of their path of flight. As defined by the U.S. Army Classifies unmanned aircraft are grouped by maximum payload. The target unmanned aircraft for this project fits into Group 2 or Group 3 which ranges from 21 to 1320 pounds (9.5 to 599 kg) [1]. Requirements from the nature of these unmanned aircraft insist that payload components, such as a sense and avoid system, be of low size, weight, and power (SWaP). Dr. Krouglicof proposed a system in which an intelligent camera would have a fixed field of view and be able to identify airborne objects within that field of view, this will then provide the unmanned vehicle with the ability to locate the object in two dimensions, however to be able to navigate around or away from an object all three dimensions are needed. In order to determine the depth of the object a second sensor must be used. It was proposed that a precise high-speed pointing device would be used to move this sensor and gather the depth information.

Typically, in opto-electric aircraft payloads a gimbal based turret system is used, such as the TASE150 [2], or MicroPOP [3]. Although these systems can be very accurate, they can consume large amounts of power, be slow moving, and heavy. As an alternative the project aimed to create a high speed parallel kinematic mechanism (PKM). A PKM has many advantages over a gimbal, as it has a much lower moving mass, therefore requiring less power, and is able to achieve faster speeds. Another alternative to a gimbal or a PKM is a fixed radar system which can scan an area for objects such as the EchoFlight [4]. This provides a convenient package solution with no moving mass, however has a fixed field of view and limited repetition rate. A comparison of specifications of gimbal systems performance and a radar solution can be found in Table 1. The project group developed a high-speed linear motor based on voice coil technology that is capable of sub-micron precision, a velocity of 2 meters per second, and a 6.6 newton per amp force constant within a 12-millimeter stroke. This was then used in a unique robotic architecture to create two unique PKM devices, one able to move in two degrees of freedom, and the other in three degrees of freedom. These two devices weigh less than 2.5 kilograms and are able to achieve over 1000 degrees per second pointing speed in any direction, maintain a pointing accuracy of a one hundredth of a degree, and only consume on average seven watts of power. With a pointing device capable of moving to a new position every 20 milliseconds, it was determined that the sensor needed to solve the sense and avoid problem would be a time-of-flight laser rangefinder with a high repetition rate. In comparison to using a second camera for gathering depth information, a time-of-flight laser rangefinder can gather information at a much higher rate, while maintaining SWaP requirements.

Table 1: Comparison of Gimbal Systems and PKM

Specification	**PKM+LRF**	**TASE150**	**MicroPOP**	**EchoFlight**	**Units**
Pan	+/- 32	360	360	120(fixed field of view)	Degrees
Tilt	+/- 32	+23/-203	+30/-90	80(fixed field of view)	Degrees
Yaw	+/- 32	N/A	N/A	N/A	Degrees
Rotation Rate	630(average) - 1170(max)	150	100	N/A	Degrees/ Sec
Power	0.54(min) - 8(max)	14 (average) - 22(max)	15-16.8	15(Standby) - 40(Operating)	Watts
Size	137x137x148	122x112x178	104x104x180	187x121x40	mm
Weight	2.15	0.9	1.2	0.73-0.817	kg

1.2. Design Requirements

With the determination that a time-of-flight laser rangefinder was needed for the sense and avoid system, certain design requirements were identified. Table 2 provides a summary of all design specifications explained in this sections. Based on the settling time for the pointing device it was found that a repetition rate of at least 50 measurements per second was required. The pointing device is capable of moving from one position to another anywhere within the working envelope in 20 milliseconds, therefore a repetition rate of 50 measurements per second would align with this constraint. The pointing device also strictly determines the physical dimensions of the rangefinder. As the performance of the pointing device is affected greatly by the mass of the object mounted on the motion platform, the laser rangefinder cannot exceed a mass of 250 grams. In addition to the affect of mass on the performance of the pointing device, the inertia of the rangefinder must be minimized; this corresponds to the mounted height being kept at a minimum. As well, due to the physical structure of the pointing device the rangefinder must fit within a circular area 65 millimeters in diameter.

As part of the Intelligent Sensor Platforms for Unmanned Vehicles project a controller board was developed using a Field Programmable Gate Array (FPGA). This controller board was used for every device developed within the project in order to ensure cohesive operation between devices. Therefore, to maintain consistent development this same board must be used for the development of the laser rangefinder. Utilizing this board will aid in maintaining the SWaP requirements of the sense and avoid system as both the pointing device and rangefinder can operate through the same controller board, simplifying the overall design and minimizing the maximum power used. The use of this board will also help in communication between the pointing device/rangefinder controller and the controller of the intelligent camera, which will also be using a board of the same design.

A critical constraint that is required for the rangefinder is that of the useable range. As it is intended to be used for a sense and avoid system, measurement at a range of less than 50 meters is not necessary. The targets of interest and unmanned vehicle itself will be moving at speeds ranging from 50 meters per second to upwards of 250 meters per second; therefore within 50 meters it would be too late for a maneuver to avoid collision. The distance of interest is on the order of 1 kilometer, providing the unmanned vehicle significant time to maneuver out of a collision path. At this distance the accuracy design constraint is less than or equal to 1 meter.

Table 2: Design Specifications

Design Specification	Value
Max Diameter	65 mm
Maximum Weight	0.25 kg
Repetition Rate	50 Hz
Measurement Range	50 – 1000 m
Accuracy	< 1 m
Power Supply	12V

1.3. Objectives and Expected Outcomes

Objective 1: Develop custom optical interfaces for laser rangefinder.

- Outcome 1: An algorithm capable of producing lens profile for collimating light from a laser diode.
- Outcome 2: An algorithm capable of producing a mirror profile able to focus ambient light to a known point.

- Outcome 3: Experimental evaluation of custom designed and manufactured optical interfaces.

Objective 2: Development of electrical system for laser rangefinder.

- Outcome 4: Hardware implemented pulsing circuit able to meet design requirements.
- Outcome 5: Hardware implemented receiving circuit able to meet design requirements.
- Outcome 6: FPGA based controller for interfacing with laser rangefinder.

Objective 3: Development of mechanical structure for laser rangefinder

- Outcome 7: A manufactured laser rangefinder housing meeting design requirements.

1.4. Thesis Outline

Chapter 1: Introduction – This chapter provides background context to the thesis and defines objectives for the project.

Chapter 2: Literature Review – This chapter provides a summary of the advancement of laser rangefinder technology.

Chapter 3: Optical Design – This chapter outlines the algorithms developed to create the optical system of the laser rangefinder, relating to the first objective and outcomes.

Chapter 4: Electrical Design – This chapter details the design and testing of the electrical systems of the laser rangefinder.

Chapter 5: Mechanical Design – This chapter specifies all mechanical components required to assemble the laser rangefinder.

Chapter 6: FPGA Design – This chapter specifies the development of the control algorithm for the laser rangefinder.

Chapter 7: Conclusions – Provides a summary of the thesis and outcomes of the objectives.

Chapter 2: Literature Review

2.1 Laser Rangefinders

In the late 1950's the ruby laser was invented, paving the way for many further developments. One such development was the invention of the laser rangefinder. In 1961 the first laser rangefinder was developed, demonstrating the capabilities of the ruby laser. This system however weighed 90 pounds. Shortly after, in 1966, in the paper "The Laser Rangefinder", Hamilton and Fowler describe a portable laser rangefinder system capable of ranging 10 kilometers with an accuracy of 10 meters, weighing 35 pounds [5]. By the late 1960's development of Gallium Arsenide (GaAs) injection lasers were successful, which provided new methods for laser ranging [6]. The main benefits to the GaAs laser were the improvement on overall size and weight in comparison to the ruby laser, as well as high pulse repetition rate. With this configuration, a laser rangefinder was developed where the total weight was only 9 pounds, 10% of the first laser rangefinder although the ranging distance was limited to 400 meters. This range finding system described by Koechner, [6], utilizes a coaxial optical arrangement where the receiving optical axis is in line with the transmitting optics. This design is achieved through the use of a classic Cassegrain telescope where the incoming parallel light rays are reflected off of a parabolic mirror onto smaller hyperbolic mirror centered in the telescope. The hyperbolic mirror reflects the light rays back to a focal point behind the telescope body [7]. This telescope design has been in use since the 1700's when described by Cassegrain and Newton. This arrangement is popular for maintaining a long optical path in a compact physical size. The described laser rangefinder places the transmitting laser in front of the hyperbolic mirror, therefore not detracting from any received light, and the receiving unit is placed behind the Cassegrain telescope collecting light through the focus of the hyperbolic mirror. This design also utilizes a beam splitter to reflect visible light to a viewfinder for manual positioning. This beam splitter allows the infrared light from the transmitter to pass into the receiving unit [6]. Even into the 1980's GaAs lasers were still limited to ranging on the order of 100 meters, the common approach for longer range remained pumped lasers [8], although no longer ruby, typically Nd:YAG.

To show the progression that has been made in laser diode technologies, it can easily be seen in the 21st century that laser diode rangefinders are readily available at low cost. These devices can be purchased commercially for uses such as hunting and golfing such as the Bushnell Legend Rangefinder [9]. This is a point and shoot laser rangefinder capable of 1000-meter maximum range on a reflective target for a price of 184.00 USD. In an industrial market, Jenoptik offers laser diode rangefinders with maximum ranges of 20,000 meters [10]. These two examples demonstrate the advancement in laser diodes and electronics in the last 30 years and a summary of the performance characteristics can be found in Table 3.

Table 3: Specifications of Commercial Laser Rangefinders

Design Specification	Bushnell Legend	Jenoptik DLEM	Units
Size	33x107x74	97x25x50	mm
Weight	0.17	0.095	kg
Repetition Rate	N/A	1	Hz
Measurement Range	5 - 1097	10-5000	meters
Accuracy	0.9	1	meters
Power Supply	3	10	Volts

This technology has been further developed into many different forms and uses. In addition, the methods of Laser Range finding have broadened as range can be determined based on time of flight sensors, measuring the time it takes for a laser pulse to travel to and from a target, or the phase shift of a reflected laser pulse can be examined to determine the range. Applications of this technology have been used to create devices that can collect data of thousands of points simultaneously, one single point over vast ranges, or a single point over a very short distance at high precision. The uses for the laser rangefinders can be found in both military and civilian applications.

2.1.1 Ranging Method

There are two main types of laser ranging methods, time-of-flight and phase shift, also known as phase modulation. Each of these ranging methods have different strengths and weaknesses and are used for varying applications.

Time-of-flight laser rangefinders utilize time measurement as the source of distance measurement. The main principal is to time how long it takes a laser pulse to travel from the source, reflect off of the target, and return to the detector located close to the source. This type of laser range finder excels at ranging objects at large distances, upwards of 1 kilometer, while maintaining minimal power consumption. The key factors to time of flight are ensuring a narrow high-power pulse and a high rate of counting to maintain precision. In the first laser rangefinders the method in which these lasers were able to create high power short pulses was through utilizing Q-switching [11]. Q-switching refers to a technique where laser energy is stored and then released instantaneously in order to produce high power laser pulses [12]. Q-Switching was completed through various means including, mechanical, acousto-optic, electro-optic, or dye switching. An example of mechanical Q-Switching is the use of a rotating mirror which would shutter the laser light as it leaves a resonating chamber. Utilizing mechanical methods presented problems due to size and weight limitations, as well as the maintenance on the device [11]. With advancement in semiconductor lasers there are many benefits as they are small and efficient and do not require the Q-Switching methods found with traditional lasers. In place of the Q-Switching methods, a semiconductor laser can be pulsed with the drive current [8]. This ability significantly improves portability and maintainability of the laser rangefinder. The counting resolution of early laser rangefinders consisted of analog counters, an example of which is described by Koechner. The analog counter consists of a bistable multibibrator, integrating RC network, and four monostable multivibrators for reset conditions. This counter is triggered by the transmission voltage of the laser and stopped by the reception of the pulse or monostable multivibrators. The output of the integrating element is fed into an amplifier which provides the signal to a panel meter [6]. Advances in electronics allowed for the development of digital counters which utilize a crystal-controlled clock for counting. This method makes the resolution of the measurement directly related to the clock frequency; a higher frequency provides a higher resolution. With the development of FPGA devices, the counter and control method can be housed in a single device with small footprint compared to the 4 cubic inch size of an analog counter.

An FPGA, or Field Programmable Gate Array, is a form of application specific integrated circuit that has several thousand usable gate arrays that can be reprogrammed [13]. This ability provides an opportunity for rapid prototyping and development for small volume ASICs. Specifically of use in an FPGA is the ability to create multiple clocks at varying speeds through a phase lock loop (PLL) [14]. Based on the clock of the system, a PLL can be generated through means such as multiplying or dividing the system clock, for a laser rangefinder, this allows a transmitting pulse frequency and timing frequency to both be generated through the same controlling device, providing synchronization of the start points for the transmission and counter. In addition, the PLL can be scaled to the maximum available limit of the FPGA to provide optimum timing resolution.

Phase shift rangefinders function under a different principal than time-of-flight sensors. In order to determine distance, they emit a source signal in the form of a sine wave and modulate the frequency and amplitude of the sine wave. The modulated sine wave is reflected off of the target and the returning signal is captured. The reflected wave will have undergone a phase shift, where the peaks of the sine wave now occur at a different point. The size of the phase shift is then correlated to a distance [15]. Primary uses for this type of method include point cloud generation, where an entire scene is to be captured in a short period of time, such as in architectural heritage scanning [16]. As phase shift rangefinders must emit a constant signal, the power consumption is higher than time-of-flight sensors, and the range is limited to the power available.

Chapter 3: Optical Design

3.1. Introduction

Through the required constraints on the laser rangefinder for size, weight, and power, it was decided that an infrared laser emitting diode would be used as the optical power source. A laser diode was selected based on the optical power output, package size, and maximum pulsing rate. The laser diode that was chosen was the OSRAM Semiconductor SPL PL 90_3. This laser diode is capable of a maximum optical output power of 90 Watts with a wavelength of 905n. It is housed in a standard five-millimeter diode package and is capable of generating laser pulses from 1 to 100 nanoseconds in length. There were no other laser diodes that provided comparable performance in this package. In conjunction with the infrared emitter, the Panasonic PNZ331CL PIN Photodiode was chosen as the optical receiver. This receiver meets all size, weight, and power requirements, and a two nanosecond rise and fall time. The benefit of the rise and fall time will aid in producing accurate return signal identification.

A unique novel arrangement was developed for the laser rangefinder in which all optical components would exist along the same optical axis. This would be achieved by developing a combined lens which will provide collimation for the laser diode while allowing the returning light to pass unaltered through the surrounding area. A focusing mirror is positioned at the end of the laser rangefinder to direct the returning light onto the photodiode. Utilizing this coaxial design provides improved alignment of the transmitting and receiving light paths, as well as opportunities to minimize the overall size as a single lens can be used for two purposes, as opposed to two separate lenses. A generalization of the coaxial operation of the laser rangefinder can be found in Figure 1, showing the light path of both the transmitted light and received light though the same lens.

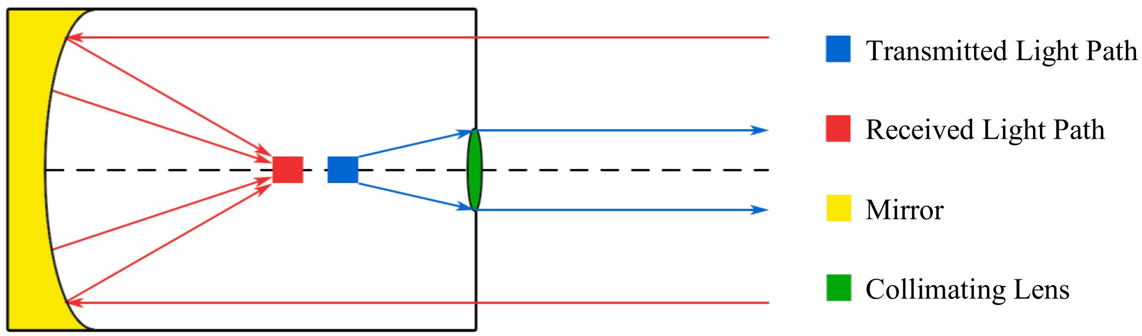

Figure 1: Coaxial Laser Rangefinder Light Path

3.2. Development of Ray Tracing Algorithm for Design of Aspherical Optical Interface

Ray tracing is based on the assumption that light can be simplified into straight lines that pass through an optical interface undergoing operations of refraction or reflection to produce the resultant image [17] . Using this simplification and known light characteristics, an algorithm can be developed that will define the shape of a lens that is required to achieve a desired light image. In the case of a laser rangefinder an algorithm must be made to define a lens with an image that is a spot of collimated light, light rays that are parallel, and a second algorithm to define a mirror that can focus collimated light to a specific point.

To begin developing an algorithm, the desired light path must be identified. This may be due to physical constraints on the size of the lens, or light source characteristics. For the case of a light source, a technical specification sheet can be used to determine the maximum angle at which light is emitted, therefore providing a maximum ray angle that a light ray will follow. This also determines the maximum diameter of the lens, as the diameter will become a function of the largest ray angle and focal length, or distance from the lens. With the light source known we can define each ray graphically by the linear equation as shown in Equation 1, where y and x are the radius of the lens and distance along optical axis on a graph, m is the slope of the line, and b is the y-intercept.

$$y = mx + b \qquad \textbf{Equation 1}$$

In the design of a singular lens, it is known that there will be two optical interfaces, the first being the intercept of the ray with the lens after it has left the light source and the second as the ray passes from the lens back into the atmosphere. With two optical interfaces there will be three different ray line equations, the first being simplified with the assumption that the origin will act as the light source, removing the y-intercept (b=0), and the third equation can be simplified to a constant as it is known that the light will be collimated. As the second ray equation has no specific definition, it must be constrained. This can be completed by specifying a desired angle change between the first and second ray. For this algorithm it was chosen that the angle would be reduced by half. The graphical representation of this is conveyed in Figure 2.

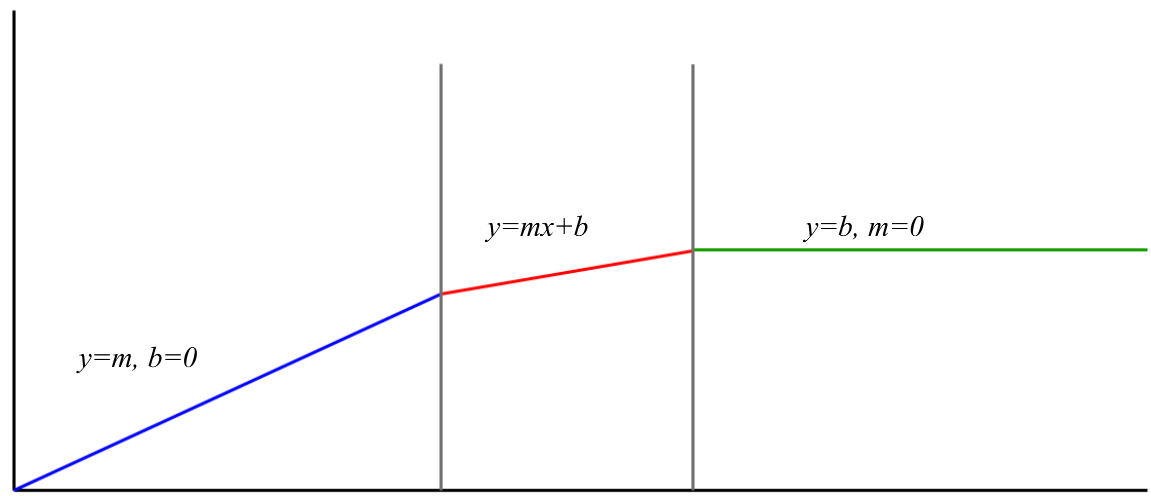

Figure 2: Graphical representation of ray angle change

With a known ray line slope throughout the lens, we must determine where the lens interface is, this can be done by creating a parameter for the distance to the first interface, called effective focal length (EFL). This defines the distance from the light source to the first interface along the x-axis. In order to define the second interface a parameter is created for the thickness of the lens, as defined by the distance between the first and second interface along the optical axis, or x-axis. With a known position of the optical interfaces along the optical axis the intersection points between the ray lines and the optical interface can be determined. In order to determine the intercept, the equation of a line can be identified that follows a path between the desired intercept and the previous intercept with a slope identified by Snell's Law. It is also known that this point is an intercept for the refracted ray.

With the design constraints of the ray paths and mediums in which the ray will be passing known, the required slope for the optical interface along each ray can be identified through the application of Snell's Law, Equation 2 Snell's Law dictates that the relation of the sines of the input and output ray angles will be proportional to the relation of the index of refraction of the mediums.

$$n_{in} \sin(\theta_{in}) = n_{out} \sin(\theta_{out}) \qquad \textbf{Equation 2}$$

As Snell's Law is applied to a flat plane, entry and exit angles are defined relative to the normal of that flat plane, therefore we can determine the slope of the flat plane, which is a tangent on the lens interface at the intersection point of each incoming and outgoing ray line, and the coordinates of the intersection point on this plane. To do this each ray line slope must be converted to an incident angle to the tangent, and the angle of the normal to the tangent must be identified in order to relate the slope of the tangent back to the axis.

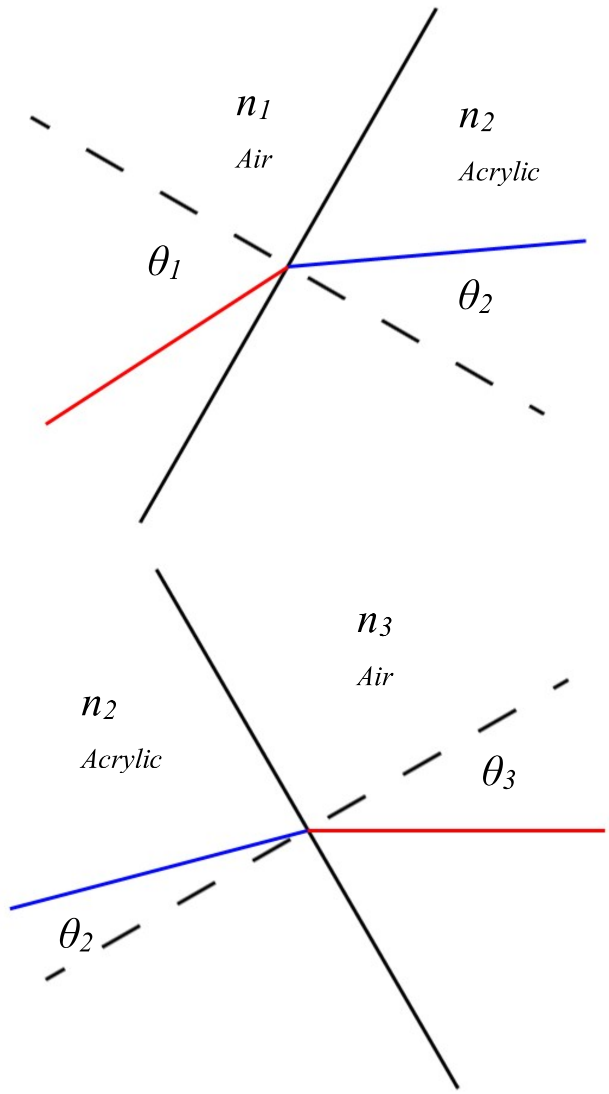

Figure 3: Snell's Law Example (First Interface left, Second Interface right, Air side red, Acrylic side blue)

It is also known that based on the design constraints of moving from a larger to a smaller slope (angled ray from the source to parallel collimated rays), and that the index of refraction of the lens medium is greater than that of atmosphere, the first lens interface will consist of tangents of decreasing positive slope values and the second interface will be increasing negative slope values, moving through the horizontal optical axis, therefore simplifying the formulas required in the algorithm.

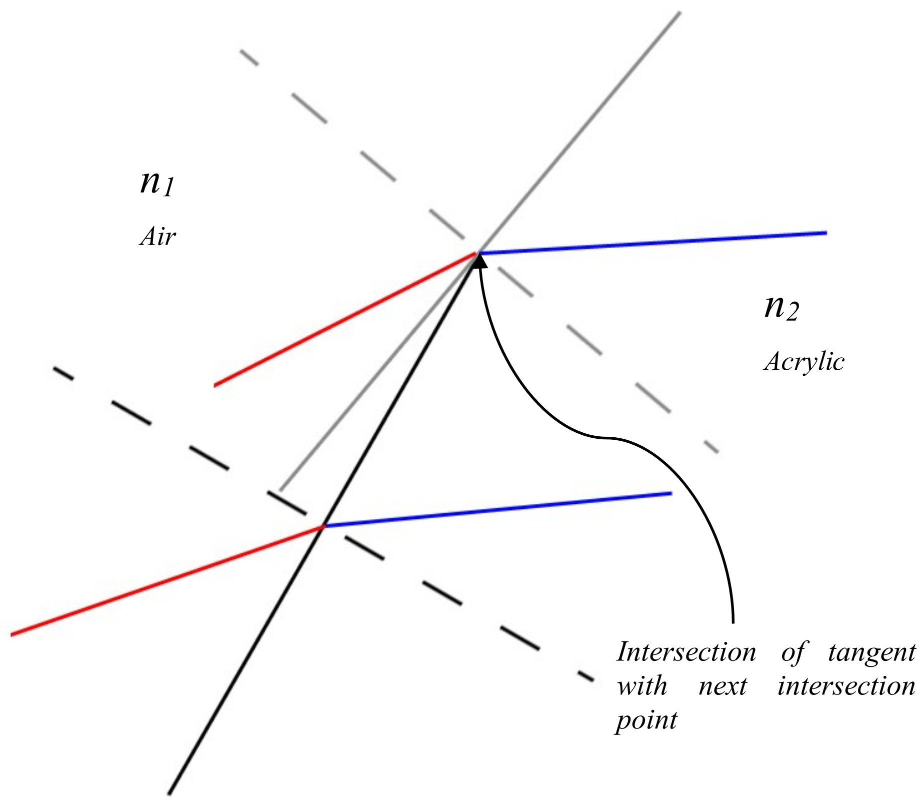

Figure 4: Lens Extrapolation Diagram

For a known slope of value m, the angle between the slope and the horizontal can be defined by the arctan of m. If the design optical axis occurs on the x-axis, the angle between the first ray and first interface would be equal to arctan of m, α, plus the angle between the normal of the tangent and the horizontal, β_n,

Equation 3.

$$\theta_{in} = \beta_n + \alpha \qquad \textbf{Equation 3}$$

In the case of the first interface it is known that the outgoing angle will be equal to half of the incoming angle relative to the horizontal, γ, as specified by the design constraints, plus the angle between the normal of the tangent and the horizontal, β_n as described in Equation 4.

$$\theta_{out} = \beta_n + \gamma \qquad \textbf{Equation 4}$$

Utilizing Snell's Law, Equation 2, a new equation can be created by substituting the constraints for the incoming and outgoing angles as described in Equation 3 and Equation 4. This substitution creates Equation 5 which can be used to solve for β_n through the use of the Newton –Raphson method.

$$n_{in} \sin(\beta_n + \alpha) = n_{out} \sin(\beta_n + \gamma) \qquad \textbf{Equation 5}$$

Newton-Raphson method is an iterative method in which a function is specified, in this case the function found in Equation 6 is equivalent to Equation **5** rearranged.

$$F(\overline{\beta_n}) = n_{out} \sin(\overline{\beta_n} + \gamma) - n_{in} \sin(\overline{\beta_n} + \alpha) \qquad \textbf{Equation 6}$$

Newton Raphson method requires an initial guess of the value of β_n, then increments this value of β_n, by a value determined by dividing the solution of the original function, Equation 6 at the initial guess, by the derivative of the function Equation 7 at the initial guess.

$$F'\left(\overline{\beta_n}\right) = n_{out}\cos\left(\overline{\beta_n} + \gamma\right) - n_{in}\cos\left(\overline{\beta_n} + \alpha\right)$$ **Equation 7**

Dividing the original function by the derivative, which is equivalent to the slope of the function at the estimated value, a delta value is identified, d_{th}, as shown in Equation 8.

$$d_{th} = \frac{-F\left(\overline{\beta_n}\right)}{F'\left(\overline{\beta_n}\right)}$$ **Equation 8**

The delta value, d_{th}, is used to increment the value of β_n until the delta value is near zero, defined by 10^{-6}. The iteration equation for β_n is found in Equation 9.

$$\overline{\beta_{n+1}} = \overline{\beta_n} + d_{th}$$ **Equation 9**

With the solution of the Newton-Raphson method producing a value of β_n, the normal of the curve of the lens, Equation 10 defines the slope of the tangent to the curve by taking the inverse of the tangent of β_n.

$$m_{\tan} = \frac{1}{\tan(\beta_n)}$$ **Equation 10**

With the slope of the tangent at the intersection of the ray and the optical interface known, starting with the known x intercept, EFL, Equation 11 allows a line to be defined between the previous intersection point and the current intersection point with the slope of the tangent.

$$y_{\tan 1} = m_{\tan 1}(x - x1_{i-1}) + y1_{i-1}$$ **Equation 11**

With known initial conditions, Equation 12 defines the equation of a ray line emitted from the light source; therefore, the y intercept of this equation is equal to zero.

$$y_{ray} = mx$$ **Equation 12**

With defined equations for a ray emitted from the source, Equation 12, and a line along two points of the lens, Equation 11, Equation 13 can be created by setting these equations equal to solve for the x value of the intersection of these two lines.

$$x_{\text{int} 1} = \frac{y1_{i-1} - m_{\tan 1} x1_{i-1}}{m - m_{\tan 1}}$$ **Equation 13**

With a defined equation for the x value of the intersection point an iterative method can be used to increment the value of x until it matches the calculated value of the x intercept. Simultaneously through this iterative method Equation 11 determines the y value of the intercept. It is then that both x and y values are assigned to a matrix and stored as coordinate points on the lens curve.

To calculate the coordinates of the intersection points of the second lens interface the same Newton – Raphson function is used. The only difference is that arguments are passed into the function which describes the path of the ray entering and exiting the second interface, as constrained by design assumptions. The output of the Newton-Raphson method provides the Normal of the second interface at the intersection point with the ray which has been refracted by the first interface. Using the same method as found in Equation 10, the slope of the tangent to the second interface is identified, m_{tan2}. Equation 14 utilizes the known slope of the curve at the intersection point to define a line between the intersection point and the previous intersection point.

$$y_{\tan 2} = m_{\tan 2}(x - x2_{i-1}) + y2_{i-1} \qquad \textbf{Equation 14}$$

With the design constraint on the slope of the ray leaving the first interface, and knowing that it intersects the first lens at a defined coordinate, Equation 15 defines the path of the ray line that exits the first interface after it has undergone the refraction defined by Snell's Law.

$$y_{ray2} = m_2 x + x1_{i-1}(m - m_2) \qquad \textbf{Equation 15}$$

In a method similar to that used for the first interface Equation 14 and Equation 15 can be set equal to one another to create Equation 16, which has been rearranged to solve for the x coordinate of the intersection point of the second interface.

$$x_{\text{int}2} = \frac{y2_{i-1} - m_{\tan 2}x2_{i-1} - x1_{i-1}(m - m_2)}{m_2 - m_{\tan 2}} \qquad \textbf{Equation 16}$$

Through the same iterative process used to identify the coordinates of the first interface, the values of the x and y coordinates of the second lens interface are also captured and assigned to a matrix. This is then repeated for a defined number of iterations to generate a series of points which can be used to determine the polynomial of the curve of the first and second interfaces through regression.

3.3. Development of ray tracing algorithm for lens validation

With a completed lens design through the algorithm defined in section 3.2, or any other lens defined by a polynomial, an algorithm can be developed that computes the effectiveness of the lens for the use of collimation. This algorithm begins with specific assumptions; that the transmitting source is known, and that it will originate at a known distance, or within a specified range of distances from the first lens interface and that the polynomial of the lens interfaces is defined. The purpose of the algorithm is to output a series of ray angles emitted from the second lens interface and determine how closely they resemble that of fully collimated light rays.

Similar to section 3.2 Newton – Raphson method can be used, however in this case, instead of solving for the normal to the curve, it will be used to solve for the coordinates along the curve in which the ray and the curve intersect. As the polynomial is known, the outgoing ray angles from both the first and second interfaces can be solved directly with the solution of Newton Raphson. To solve for the x and y coordinates of the intersection point, the algorithm utilizes the slope of the ray exiting the light sources as an input, incrementing the slope, and therefore angle, across the first lens interface. Equation 17 defines the equation of the ray emitted from the source with input slope *m,* with a y-intercept value equivalent to the effective focal length, EFL, of the lens, or distance of the emitter from the first lens interface.

$$y = mx - EFL \qquad \textbf{Equation 17}$$

To complete the function for Newton-Raphson the polynomial of the lens interface must be defined. Equation 18 defines the polynomial of the first lens interface, the constants A, B, and C are inputs of the algorithm.

$$y_1 = A_1 x^2 + B_1 x + C_1 \qquad \textbf{Equation 18}$$

With both the equation of the incoming ray and the polynomial of the first interface defined, Equation 19, the Newton-Raphson function can be defined as a matrix of the two equations with two unknowns.

$$F(\bar{x}, \bar{y}) = \begin{bmatrix} A\bar{x}^2 + B\bar{x} + C - \bar{y} \\ m\bar{x} - \bar{y} - EFL \end{bmatrix} \qquad \textbf{Equation 19}$$

With the function defined, the derivative must be determined in order to calculate the delta values for the x and y coordinates based on the initial guess. Equation 20 defines the derivative of the function in Equation 19, also in the form of a matrix of two equations.

$$F'\left(\bar{x},\bar{y}\right)=\begin{bmatrix} 2A\bar{x}+B & -1 \\ m & -1 \end{bmatrix}$$ **Equation 20**

With the function and derivative defined, the delta value, d_{th}, of the initial guess can be determined through Equation 21, in which the function is divided by the derivative.

$$d_{th}=\frac{-F\left(\bar{x},\bar{y}\right)}{F'\left(\bar{x},\bar{y}\right)}$$ **Equation 21**

With the delta value defined, the next iteration of x and y coordinates can be determined through Equation 22 and repeated until the result of the delta approaches zero. In the algorithm this point is defined as 10^{-6}.

$$\begin{bmatrix} \overline{x_{\text{int}}} \\ \overline{y_{\text{int}}} \end{bmatrix}=\begin{bmatrix} \bar{x} \\ \bar{y} \end{bmatrix}+\begin{bmatrix} dx_{th} \\ dy_{th} \end{bmatrix}$$ **Equation 22**

With the solution of the coordinates of the intersection point of the first ray and the first interface, it is now possible to use these values to determine the path of the ray exiting the first interface. This can be done by rearranging Snell's Law to solve for the outgoing angle where the ray is moving from air to the lens medium. To simplify the equations, a substitution is made in Snell's Law, Equation 2, using Equation 23 to define the index of refraction (IOR) as the lens medium divided by the atmospheric medium.

$$IOR = \frac{n_{lens}}{n_{atmosphere}}$$ **Equation 23**

$$\theta_{O1} = a\sin\left(\frac{\sin(\theta_{I1})}{IOR}\right)$$ **Equation 24**

We know that when applying Snell's law to a ray passing through an interface the angles are relative to the normal of the interface, therefore we must determine the angle of the normal. It is known that the derivative of a polynomial is equal to the slope of the polynomial at a given set of coordinates, m_{tan1}, as described in Equation 25. With this slope identified, we can use Equation 26 defines the angle of the normal from the slope identified in Equation 25 by taking the inverse of the tan of the slope.

$$m_{\tan 1} = 2A_1 x_{\text{int}1} + B_1$$ **Equation 25**

$$\beta_1 = a\tan(m_{\tan 1})$$ **Equation 26**

With the assumptions made that the location of the light source is known the slope acts as an input in the algorithm, and therefore Equation 27 defines the angle of the ray entering the first interface, γ_1, based on the input slope, *m*.

$$\gamma_1 = a\tan(m)$$ **Equation 27**

As stated, Snell's law requires that input and output angles be defined relative to the normal of the lens interface. Equation 28 provides the angle of the ray entering the first interface relative to the normal of the first interface β_1 and Equation 29 defines the angle of the ray exiting the first interface relative to the normal of the first interface.

$$\theta_{I1} = 90 - \gamma_1 + \beta_1$$ **Equation 28**

$$\gamma_{ray} = 90 + \beta_1 - \theta_{O1}$$ **Equation 29**

With the angle of the outgoing ray defined the slope can also be determined through Equation 30. With the slope defined an equation of the path of the ray exiting the first interface can be created in the form of a linear equation, Equation 31. Knowing that this line passes through the intersection point of the first ray and the first interface it is possible to solve for the y-intercept, b_{ray}.

$$m_{ray} = \tan(\gamma_{ray})$$ **Equation 30**

$$b_{ray} = y_{\text{int}1} - m_{ray} x_{\text{int}1}$$ **Equation 31**

Having fully defined the equation of the ray exiting the first interface and having the polynomial constants of the second interface defined through inputs of the algorithm, the Newton-Raphson function previously described can be reused. The only condition is that instead of utilizing the variables for the linear question of the first ray, slope and y-intercept, now the variables for the second ray are substituted. The output of the Newton-Raphson function will provide the x and y coordinates of the intersection point of the ray exiting the first interface and the second interface.

Similarly to identifying the angle of the ray exiting the first interface, the angle exiting the second interface can be determined through Equation 32, which rearranges Snell's Law to solve for the outgoing angle where there is a transition from the lens medium back to air.

$$\theta_{O2} = a\sin\left(IOR \sin(\theta_{I2})\right)$$ **Equation 32**

Again, as Snell's Law requires all angles to be relative to the normal of the lens interface the normal to the lens must be determined at this intersection point. This can be completed by solving for the derivative of the polynomial of the second lens interface, Equation 33, which is equivalent to the slope, and then taking the inverse tan of this to provide B_2 as found in Equation 34.

$$m_{\tan 2} = 2A_2 x_{\text{int}\,2} + B_2 \quad \textbf{Equation 33}$$

$$\beta_2 = a\tan(m_{\tan 2}) \quad \textbf{Equation 34}$$

As this algorithm has the intent of determining the difference between the outgoing ray and a perfectly collimated ray, in the case of this algorithm an angle of 90 degrees, two conditions had to be generated when determining the final output angle based on the normal to the second lens interface. One in which the angle of the normal to the lens interface is greater than that of the incoming ray, Equation 35, and one in which the angle of the normal is less than that of the incoming ray, Equation 36. The angles of the normal and ray are all relative to the horizontal plane, or x axis. This is important in determining the angle of the outgoing ray relative to the horizontal for output and analysis. If the incorrect condition was used it would provide a false value of the angle of the outgoing ray.

$$\theta_{I2} = \beta_2 - (90 - \gamma_{ray}) \quad \textbf{Equation 35}$$

$$\theta_{I2} = -\beta_2 + (90 - \gamma_{ray}) \quad \textbf{Equation 36}$$

The two conditions of the outgoing ray angle can be represented in Figure 5. In this figure the solid black line is the lens interface, the blue line is the path of the ray which has exited the first interface and is passing through the second interface, the red line is the ray exiting the second interface, and the dashed line represents the normal to the second lens interface. The depiction on the left represents the case of Equation 35, where the angle of the normal is greater than that of the incoming ray relative to the horizontal. The depiction on the right represents Equation 36 where the angle of the normal is less than that of the incoming ray relative to the horizontal.

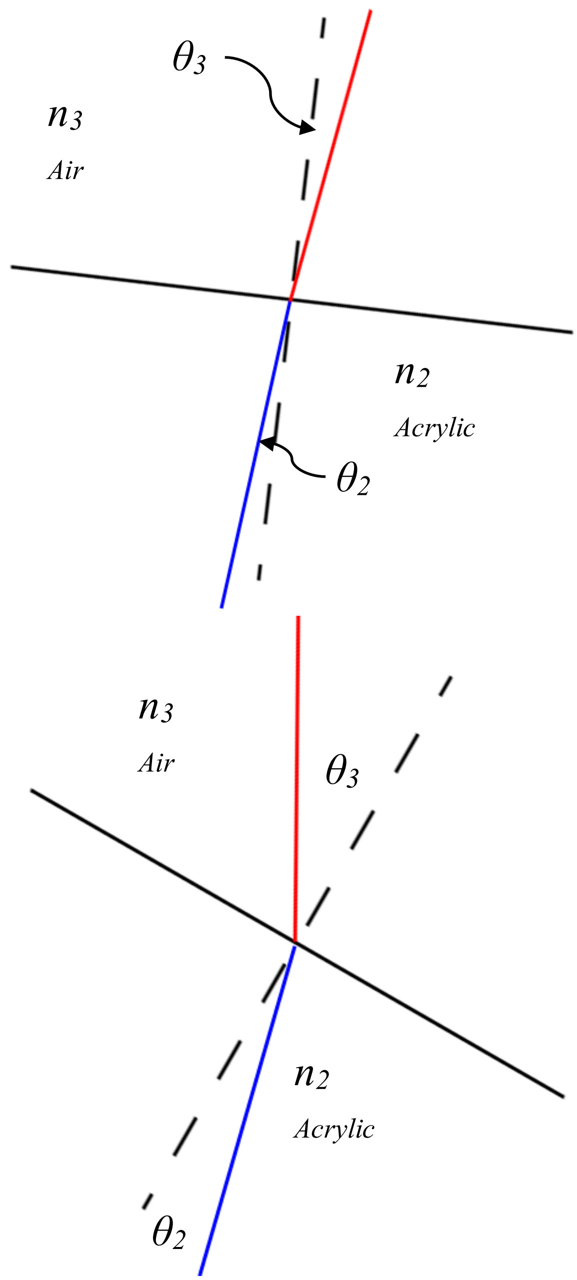

Figure 5: Representation of Equation 35 (left) and Equation 36 (Right) where the red line is the ray exiting the interface, and the dotted line is the normal to the interface

With the outgoing ray calculated, this entire process is iterated through a specified number of incoming ray slopes over a specified number for focal lengths to determine which focal length will best suit the designed lens.

3.4. Development of ray tracing algorithm for Aspherical Mirror

The development of an algorithm for an aspherical mirror was completed similarly to lens design algorithm described in section 3.2. Using the mathematical modelling software MATLAB, an algorithm was written that would determine the ideal curve for a mirror that would reflect incoming infrared light to a single point aligned with the optical axis of the mirror at a specified distance. The algorithm provides the ability to customize of the mirror shape based on the distance of the focus point from the surface of the mirror, diameter of area blocked by electronics for the receiving circuit and desired outer mirror diameter. As with the collimating lens design, incoming and outgoing ray characteristics are also known for the mirror.

For the development of the algorithm it is being assumed that incoming rays of light will be parallel with the optical axis of the mirror. This assumption has been made based on a diffuse or Lambertian reflection of the transmitted light from the target object. A diffuse reflection implies that the light energy from the transmission will be equally distributed radially outward from the point of reflection. Based on this assumption light rays will be reflected parallel to the light transmitted and return to the laser rangefinder in this pattern. Using this assumption, it is possible to define Equation 37, the path of the incoming light ray, as a constant.

$$y_{ray\_in} = b$$ **Equation 37**

The algorithm identifies the x and y coordinates of points along the mirror surface by solving the equation of the intersection of the ray of light entering the mirror and a line defined by the previous mirror point and the slope of the mirror at that point. As the ray entering the mirror is a constant parallel to the horizontal as defined in Equation 37. This value will act as an input to the algorithm and be incremented through a loop. Therefore Equation 38 can be used to make the assignment of this ray equivalent to the y value of the intersection point of the mirror.

$$y_i = y_{ray\_in}$$ **Equation 38**

Utilizing the design constraints and required inputs to the algorithm, such as distance between the mirror and the receiver and the radius at which the mirror curvature begins, the first x and y intercepts are known. With this initial condition Equation 39 can be used to solve for the next x coordinate of the intersection point of the incoming ray and the mirror.

$$x_i = \frac{y_i - y_{i-1} + x_{i-1} m_{\tan i-1}}{m_{\tan i-1}}$$ **Equation 39**

The collimating lens algorithm used Snell's Law to determine the relationship between incoming and outgoing rays of light; similarly the mirror algorithm is based on the law of reflection, Equation 40, in which the incoming angle is equivalent to the outgoing angle relative to the surface normal.

$$\theta_{in} = \theta_{out}$$ **Equation 40**

This implies that the slope of the ray relative to the normal of the intersection point of the mirror will be equivalent for the incoming and outgoing rays as represented by Figure 6. Knowing that the incoming ray is parallel to the optical axis, the horizontal, the slope of the outgoing ray is equivalent to the twice the slope of the normal. Assigning design constraints can provide enough information to specify the slope of the first ray between the focal point and the mirror can be determined. Equation 41 defines the path of a ray between the mirror and the receiver.

$$y = m_{ray}x - \frac{EFL}{m_{ray}}$$ **Equation 41**

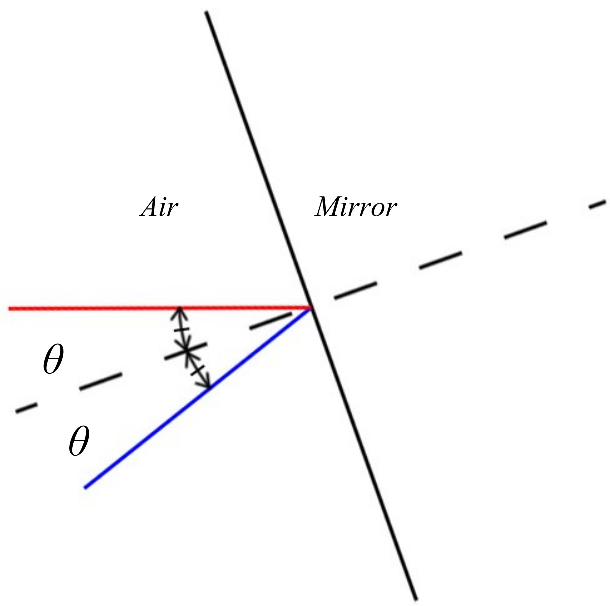

Figure 6: Representation of Equation 40, Law of Reflection

To solve for the angle of the normal Equation 41 can be rearranged to solve for the slope of the ray path between the mirror and receiver, Equation 42. Then by applying the fundamentals of the law of refraction, Equation 43 calculates the angle of the normal by finding half of the arctangent of the slope of the ray.

$$m_{ray} = \frac{y_i}{x_i - EFL} \quad \textbf{Equation 42}$$

$$\theta_{norm} = \frac{a\tan(m_{ray})}{2} \quad \textbf{Equation 43}$$

With the angle of the normal defined it is possible to identify the slope of the tangent to the mirror at the intersection point. Equation 44 shows that this is calculated by the inverse tangent of the angle of the normal.

$$m_{\tan} = \frac{-1}{\tan(\theta_{norm})} \quad \textbf{Equation 44}$$

3.5. Design of Transmitting Optics

In order to design the lens for the laser rangefinder, the algorithm described in 3.2 was written that would generate the required lens shape for specified incoming and outgoing light characteristics. As the laser diode that will be used is known, it can be assumed that the laser light is being emitted from a point source, as the emitter is quoted at 2000 square micrometers. The laser diode also specifies that the output characteristics of the laser, or beam divergence, are 9 degrees parallel to the emitter and 25 degrees perpendicular to the emitter. Therefore, using the largest beam divergence of 25 degrees, the first optical interface of the lens will have to accept point source emitting light rays at a divergence of 25 degrees. Similarly, since it is desired that the output of the lens should consist of collimated light, the light rays leaving the lens, or the second optical interface, should be parallel. With the input and output characteristics of the lens known, the only other requirements are to specify the distance of the point source from the first interface, the desired thickness of the lens, and how the light rays inside of the lens will be treated. The distance of the point source, as well as the thickness of the lens can be changed to meet the physical design requirements of the laser rangefinder.

Another required input for the algorithm is for the index of refraction of the medium in which light will pass through in order to satisfy Snell's Law. It will be assumed that the laser rangefinder will only be used in earth's atmosphere, therefore the index of refraction is 1.0 and the second medium will be acrylic, which has an index of refraction of 1.48 [18]. Acrylic was chosen as the lens material for the physical properties of clarity, weight, and machinability.

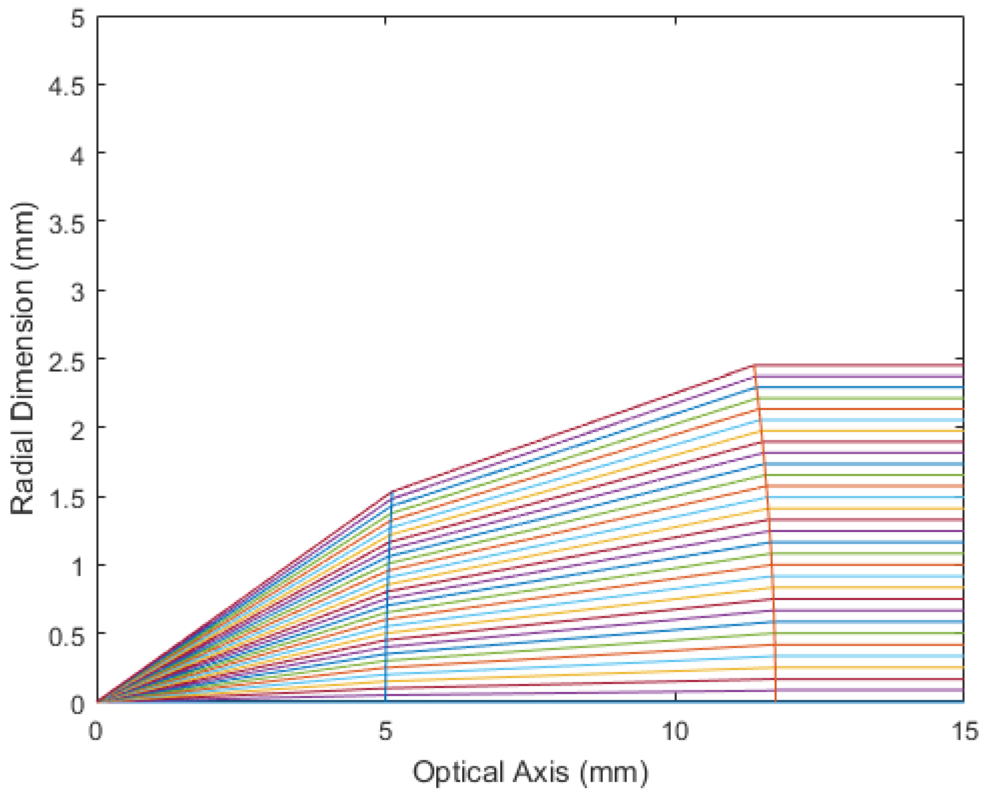

Figure 7: MATLAB Generated Lens Profile

In order to calculate the accuracy of the lens design the lens validation algorithm described in 3.3 was used. In this algorithm the angle of the outgoing ray calculated for each ray leaving the lens for a series of given focal lengths and then stored in a matrix. This matrix is then exported from MATLAB and manipulated in Excel to provide the mean square error, MSE, for each focal length. This was completed by subtracting the angle of the ray from 90 degrees to obtain the error in each ray, squaring this value and then for each focal length taking a sum of all ray errors and dividing by the number of rays as shown in Equation 45. The standard deviation of the square error was also calculated and the focal length which provided the minimum mean square error and standard deviation was identified.

$$MSE = \sum_{i=1}^{n} \frac{\left(90 - \gamma i_{ray2}\right)^2}{n}$$

Equation 45

The same process was conducted for the ray angle directly. To determine if there was agreement between mean square error and a weighted average and standard deviation of the outgoing angles distance from the ideal angle of 90. All angles were converted to radians as the design constraint was for 1 milliradian divergence, therefore 0.5 for the half lens which was studied with this algorithm. In both cases there was agreement that the ideal focal length was 7.6mm, which is 2.6 mm different than the design specification of 5mm, due to the assumptions made in the lens design algorithm. However, at this focal length the average outgoing angle is 1.57048 radians with a standard deviation of 0.00224 radians. This corresponds to an average divergence of 0.0015 radians, or 1.5 milliradians. Figure 8 and Figure 9 show the percent error across the radius of the lens comparing both the error to the outgoing ray angle and the lens profile. It can be noted that the largest error is experienced at the extremity of the lens, which is to be expected as this has the greatest ray angle transformation.

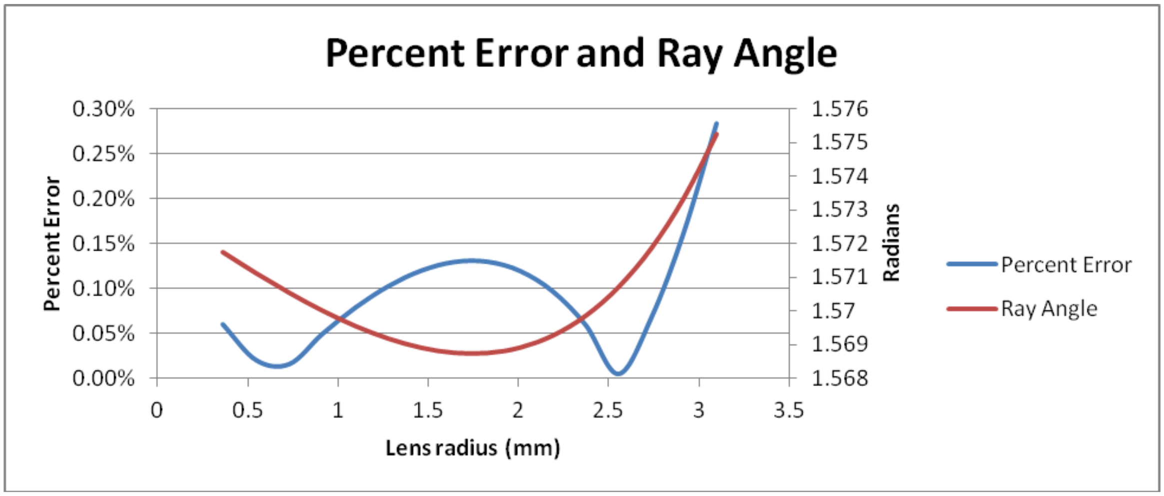

Figure 8: Percent error and Ray Angle

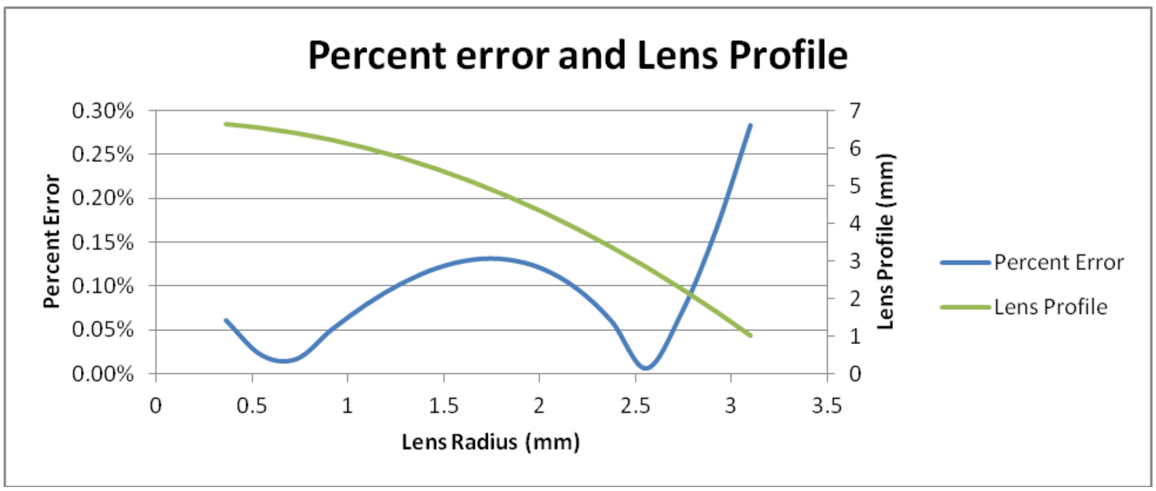

Figure 9: Percent Error and Lens Profile

3.5.1. Testing of Transmitting Optics

With the successful acquisition of data from the MATLAB code, data points were transferred into Microsoft Excel in which numerical transformations could be made simply in order to generate an equation for the profile curve centered about x and a y intercept of zero for the first optical interface and the second optical interface consisted of a y-intercept equal to the desired lens thickness specified in the MATLAB code. This equation was then transferred to the 3D Computer Aided Design software Solidworks. Utilizing the ability to create an equation driven curve in a sketch feature, the exact lens profiles were duplicated. To create a 3D part from this sketch the profiles were rotated about a central axis, collinear with the optical axis. Additional features were added to the lens in order to provide structural mounting features, as well as create the pass-through lens allowing light to reach the receiver mirror.

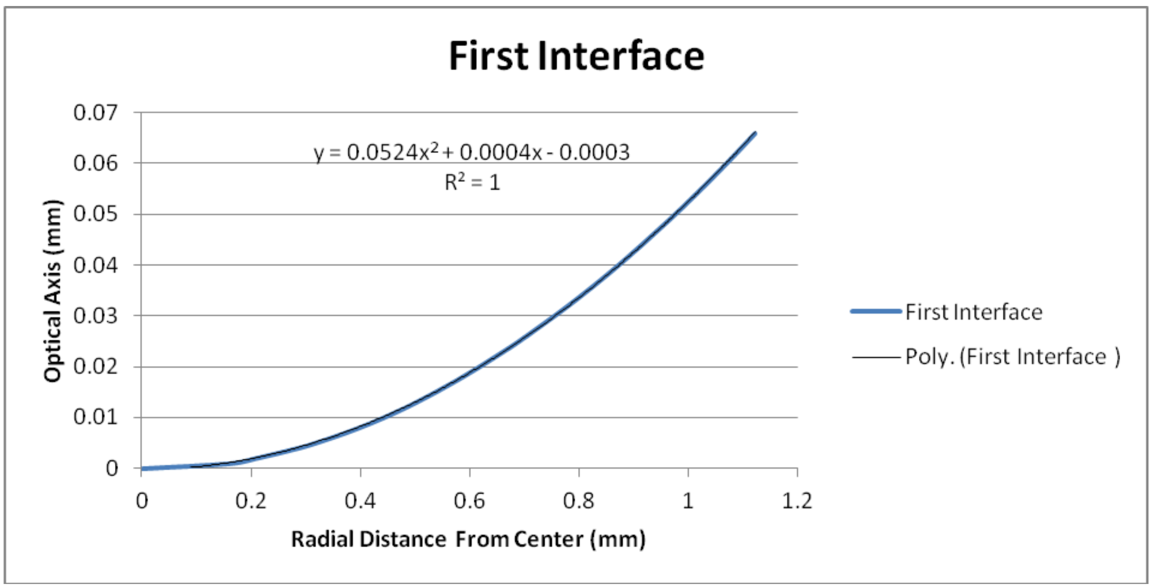

Figure 10: Polynomial Generation of First Interface

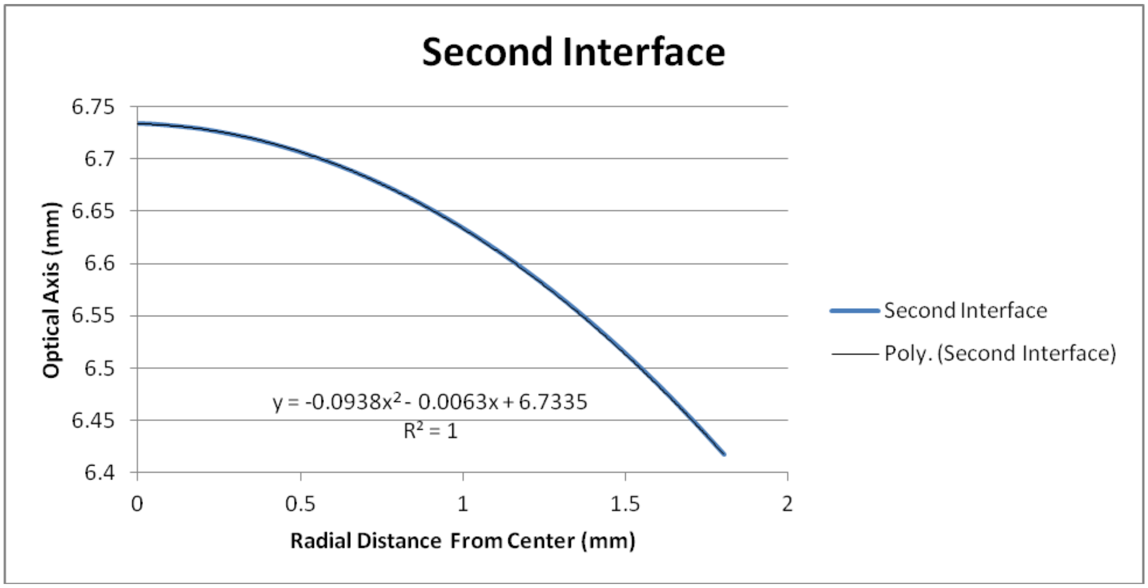

Figure 11: Polynomial Generation of Second Interface

With a completed part design, the file was then sent to a machine shop for production. Upon receipt of the completed lens a test was conducted in order to determine the accuracy of the machining process. Using the Zeiss O-Inspect Coordinate Measurement Machine in the Mechatronics Development and Prototyping Facility at Memorial University, measurements on the order of a micron were taken of the lens. Analysis of these measurements indicated that the profile that was manufactured did not match that generated in modelling software. Measurements of the lens were taken along two perpendicular axes across the second interface and the flat plane of the lens was used as a reference for a base plane. Due to the available measurement probes on the O-Inspect Machine, the first interface could not be measured. The smallest probe diameter could not measure the transition in curvature of the lens. The measurements were plotted in Microsoft Excel and compared to the theoretical curve specified by the lens design. The results indicated that the top portion of the lens appeared to be flattened, potentially from the hand polishing process and that the polynomial curve varied throughout the lens.

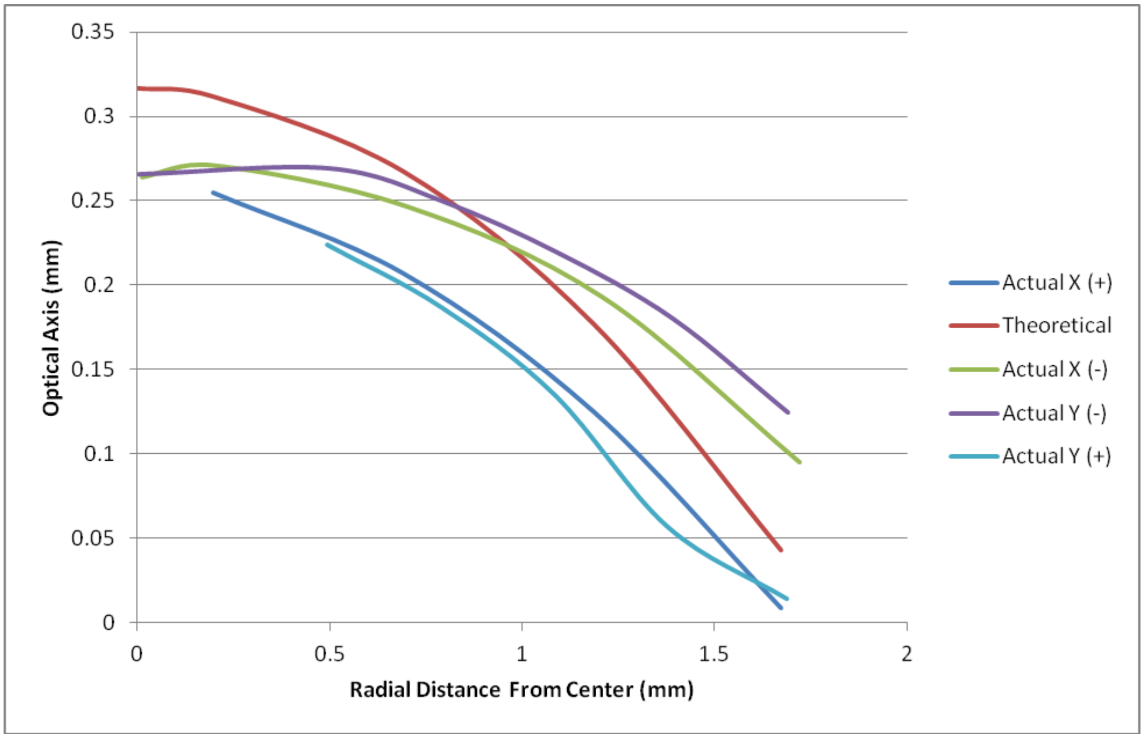

Figure 12: Actual vs. Theoretical Lens Shape

To test the optical characteristics of the lens a 3D printed mount was created to position a laser diode the correct distance from the lens. A camera with the infrared filter removed was mounted next to the lens and both were positioned facing a planar surface 2 meters away. The laser diode was set to pulse a 50ns laser pulse at a frequency of 50 hertz, while the camera had a ten thousand millisecond exposure time. At a 2-meter range a successful laser collimation lens would produce a spot approximately equal to the diameter of the collimating lens, for this case six millimeters. The spot that was captured by the camera was approximately 150-200 millimeters in diameter. When the same test arrangement was used without a collimating lens the spot size was approximately 900 millimeters along the widest axis.

Figure 13: Laser Diode Collimation Test with Machined Lens (Left) without Lens (Right)

Recognizing that it may not be feasible to produce a lens to the desired specifications, MATLAB was used to simulate what focal length would provide the optical collimating characteristics based on the measurements from the physical lens. The known measurements from the physical lens would undergo transformations in Microsoft Excel in order to generate a polynomial equation for each interface in relation to the desired configuration used to design the lens. Using the algorithm described in section 3.3, the angle of the final output ray lines and identifying the mean square error of the difference from the design target of collimated ray lines for each tested focal length, the optimal focal length can be found. Figure 14 shows the graphical output of the lens validation algorithm for a single focal length, some of the output rays appear reflected downward, however this implies that the output angle is greater than 90 degrees, or vertical.

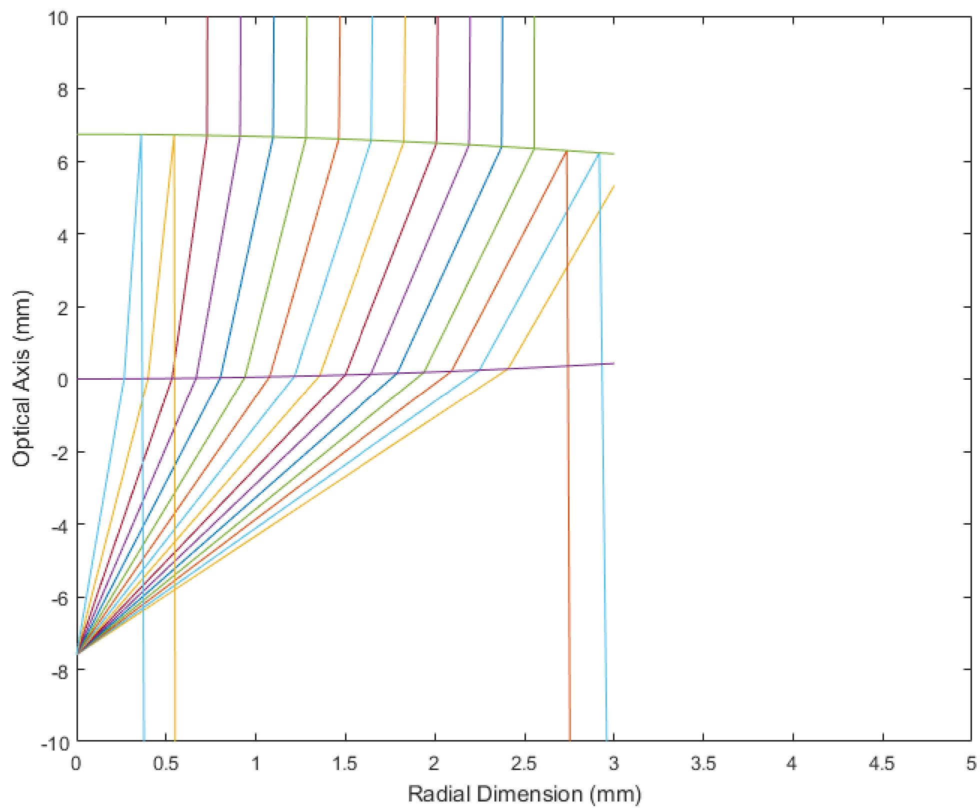

Figure 14: Ray tracing for lens validation

With the optimal focal length determined for the manufactured lens a test mount was designed using Solidworks and the Fortus 400MC 3D printer in the Mechatronic Development and Prototyping Facility. Using the known dimensions of the laser diode and the manufactured lens, the mount was designed to place the laser diode emitter in line with the optical axis of the lens, as well as the optimal focal length from the lens. With the accuracy of the Fortus 400MC it was found that the actual focal length could be guaranteed to be within 50 micron of the optimal focal length. Although an optimal focal length can be determined which minimizes the collimation losses, it may not be possible to orient the lens to provide the desired collimation characteristics. In order to determine the collimation characteristics of the lens a test was developed utilizing a camera image capture system.

The test arrangement consisted of a Lumenera Lt425 camera, accompanying software, Lucam Capture, lens test mount, lens, and laser diode. The lens and laser diode were arranged in the test mount and placed next to the Lumenera camera. The lens and camera were fixed and aligned so that the optical axes would be parallel. Both items were directed at a fixed plane, such as a wall or ceiling, with reference markings for verifying measurements on captured images. As the laser diode emits infrared light at a high rate, modifications were made to the camera and image capture settings. The infrared filter was removed from the camera and the camera lens was focused on the fixed plane. The Lucam software was used to control the exposure time and capture images. As the laser diode was pulsing and not on consistently, the exposure time of the camera was increased to 10 seconds. In addition to these changes, the test setup had to be placed in a room which could be darkened with no ambient light.

Figure 15: Lumenera Lt425

Based on standard laser collimation characteristics achieving one milliradian of beam divergence, it would be expected that if the lens performed as designed the spot size at 1 meter would be equal to the diameter of the collimating lens plus two millimeters. (tan(0.001)*1m=0.001m). With a lens diameter of approximately three millimeters, the spot size should be five millimeters. It was found that the lens produced a spot that was 110 millimeters at 1.5 meters. This value correlates to a beam divergence of 36 milliradians. As the tested beam divergence deviated greatly from that of the theoretical, it was determined that with the provided resources it was not possible to develop a customized collimating lens and that an alternative solution would have to be developed.

3.5.2. Alternative Transmitting Optics

Through design and testing it was found that due to limitations in the manufacturing processes available a feasible lens could not be produced. Future work may be completed with the implementation of precision machining practices, however, to complete the remainder of the work a standard collimating lens was purchased from Edmund Optics, lens 64-799. In order to still achieve the design requirements of collinear optical axis for the transmitting and receiving optical paths a single lens was manufactured from the purchased lens and a piece of optically clear cast acrylic. A circle of the required diameter was cut from a sheet of the acrylic with the use of a TROTEC laser cutter in the Mechatronic Development and Prototyping Facility. A hole was then precisely machined with an M9x0.5 thread at the center to receive the mount on the purchased lens. This would provide for adjustment of the purchased lens to identify the optimal focal point.

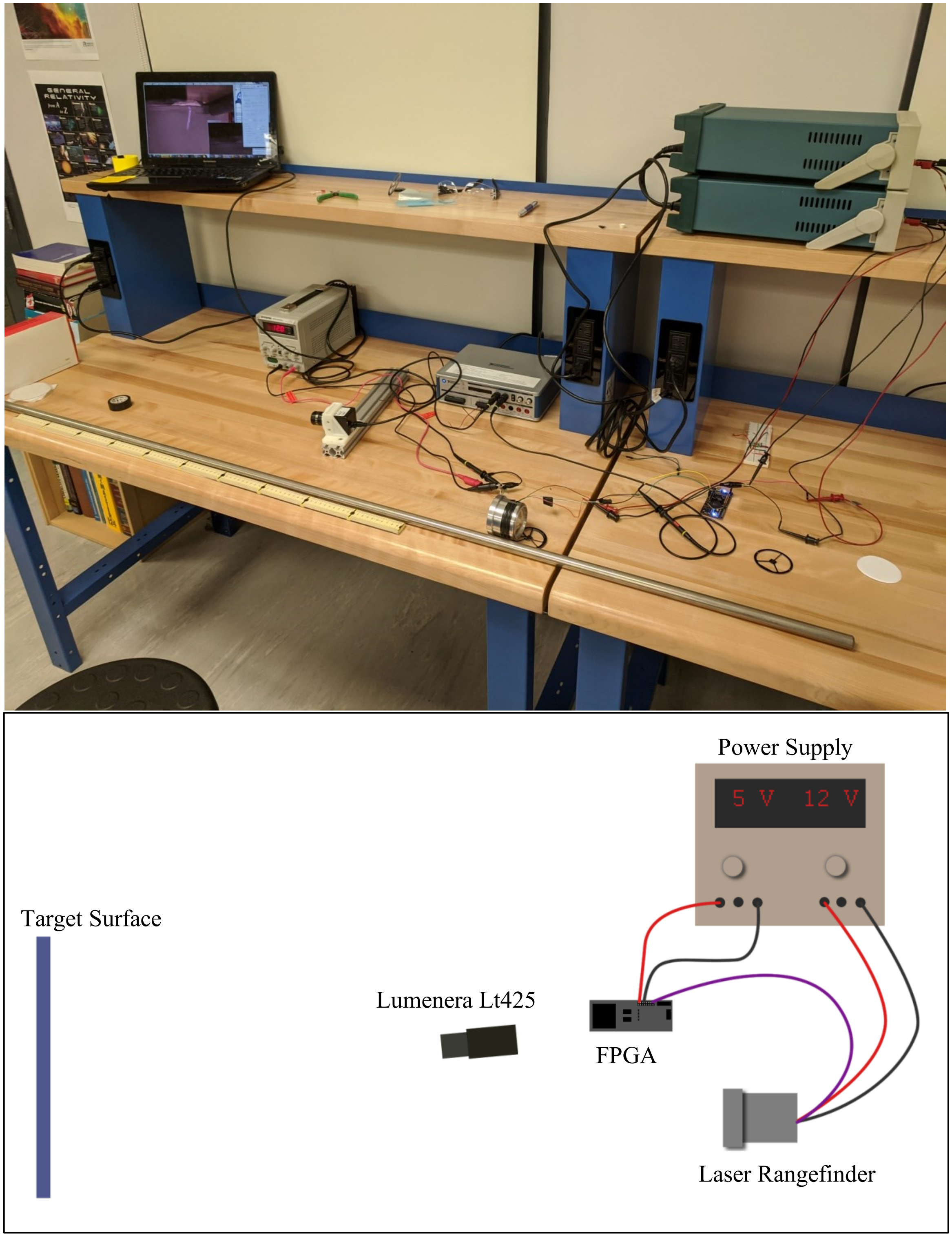

Figure 16: Laser Collimation Test Setup

To ensure proper collimation of the laser, a test setup was created with the use of a Lumenera camera. The camera would be used to detect the laser spot on an object while the focal length was adjusted, providing the ability to accurately tune the collimation. The test setup consisted of the Lumenera camera pointed at a white box, the laser rangefinder pointed at the same white box from a distance of 2 meters, the equipment required to power the laser rangefinder, and a laptop to view the camera images, as shown in Figure 16. To first ensure the functionality of detecting the infrared laser the camera was pointed directly at the transmitter and the laser was visible. The next step was to see if the laser spot could be detected on the surface of the white box. Initially, the spot was not collimated the spot was not visible with the Lumenera camera and the lab lights had to be turned off. With the lights turned off, the spot was collimated utilizing the thread on the collimating lens to identify the optimal focal length. The lights were then turned back on and the spot was highly visible as indicated by Figure 17. It can be noted that there are three distinct lines of collimated infrared light. Each of these lines corresponds to an infrared emitter found in the laser diode used in the transmitting electronics, the OSRAM SPL PL90_3. This laser diode consists of three epitaxially emitters, where three 25W emitters are stacked to create one 75W laser diode.

Figure 17: Collimated Laser

3.6. Design of Receiving Mirror

3.6.1. Light Energy Dissipation

In order to apply the lens generating algorithm described in section 3.4, a diameter of the overall mirror must be known. The size of the mirror will be restricted by the amount of light energy required by the receiver to generate a signal. Equation 46 was used to determine the size that was required for the receiving optics. This equation was defined by Nejad et al [19] and determines the amount of optical power that would be returned to the laser rangefinder receiving optics.

$$P_i = \frac{\tau A \exp(-2\alpha r)}{\pi r^2} \rho P_{opt}$$ **Equation 46**

It is required to obtain the absorption coefficient (α), or atmospheric extinction coefficient to determine the calculation of returned optical power. Wojtanoski [20] et al studied the atmospheric extinction coefficient for 905 nm lasers in the application of laser rangefinders and found that over a range of varying relative humidity, the coefficient was on average 2.3 Km^{-1} for the worst case scenario of only 1 kilometer visibility. As one of the design constraints was to achieve 1 kilometer ranging and that since the initial intention of this project was to pair the laser rangefinder with a vision system, the object targeted will need to be visible within that range. Therefore, infrared transmission through cloud and adverse atmospheric conditions can be ignored for visibility of less than 1 kilometer. It was assumed that the total transmission loss (τ) would be 0.75, as combined from the transmission medium and lens medium and that the total target reflection loss (ρ) is 1% as used by Nejad et al [19].

Using an iterative method in Microsoft Excel, the reception power was calculated for varying distances (r), optical power output (P_{opt}), and target object size. Based on the theoretical beam divergence of the designed lens, if the target object was larger than the beam, 100 percent of the beam would be returned; otherwise the reflected beam would be reduced by the fraction of the target area to the diverged beam area for the given distance. Once the returned optical power was calculated for a variety of distances, the values were then used to determine the minimum receiving optics that could be used. Similarly, the received optical energy into the laser diode would be based on a reduction of the returned light energy area and the area of the receiving optics (A), under the assumption that the designed mirror focused 100 percent of incoming light onto the photodiode. Using the datasheet from the photodiode the minimum requirement for received light can be determined, and therefore the size of the laser rangefinder can be scaled to identify a minimum size.

Although the initial design constraint was to make the laser rangefinder as small and light weight as possible to meet SWaP requirements, it was chosen to design the test laser rangefinder much larger than the minimum design requirement in order to simplify testing. The chosen mirror diameter was 50mm, this was then used in the algorithm to determine the coordinates of the mirror surface, generating the curve found in Figure 18.

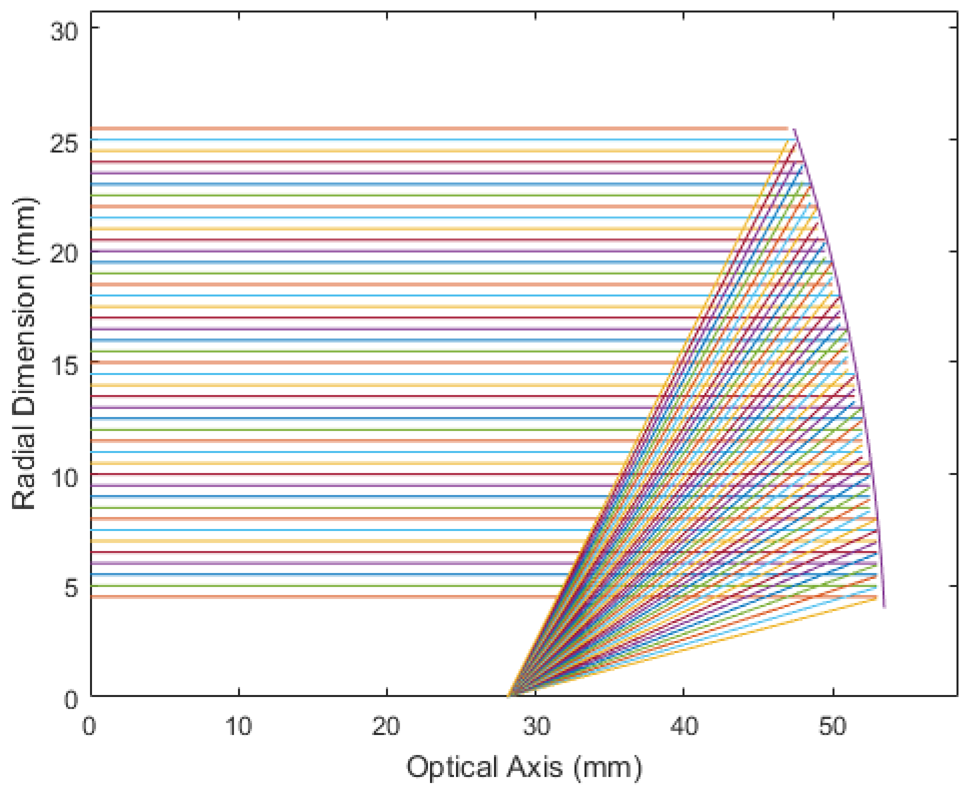

Figure 18: MATLAB Generated Mirror Profile

3.6.2. Testing of Mirror

Using the same methods as with the collimating lens, the data from the MATLAB program was transferred into Microsoft Excel. The data was then manipulated in order to fit a parabolic curve, however in this case the point of intersection with the x-axis was not at 0, but at a point equal to the radius of the specified area that was blocked by electronics. This equation was then used in Solidworks to create a 3D CAD model of the mirror. This provides the ability to add features to simplify the machining and testing processes. With a complete 3D CAD model, a drawing was created, and both the part and drawing were given to a machine shop for manufacture.

Although manufacturing flaws were identified with the production of the collimating lens, the manufacture of the mirror was attempted. As the light source is infrared light, a material would be required that is capable of reflecting the maximum percentage of infrared light. It was found that gold has a reflectivity coefficient greater than 95% for infrared light [21]. As it is impractical to manufacture the entire lens out of gold, it was determined that a gold coating could be placed on the surface of any material through the process of gold sputtering, commonly used for providing a metallic coating to non-metallic parts used in scanning electron microscopes. Therefore, aluminum was chosen as the medium for the mirror due to the ease of availability and machining characteristics. Through this method a coating of 76.7 nm thick was applied. This was completed in two coatings of 38.3nm and 38.4 nm.

Using the O-Inspect Coordinate Measurement Machine in the Mechatronics Development and Prototyping Facility the accuracy of the machining process was able to be verified. Unlike the manufacture of the collimating lens which had significant machining error, the mirror was nearly a match to the specified design and differed by an average of five percent error. It was found that the error tended to increase towards the center of the mirror. Feedback from the machinist indicated that this may be preventable with slight changes to the design of the mirror. The design included a flat portion at the center where the mirror is blocked by electronics. This provided difficulty for the tooling to continue the required radius where the curve met the flat point.

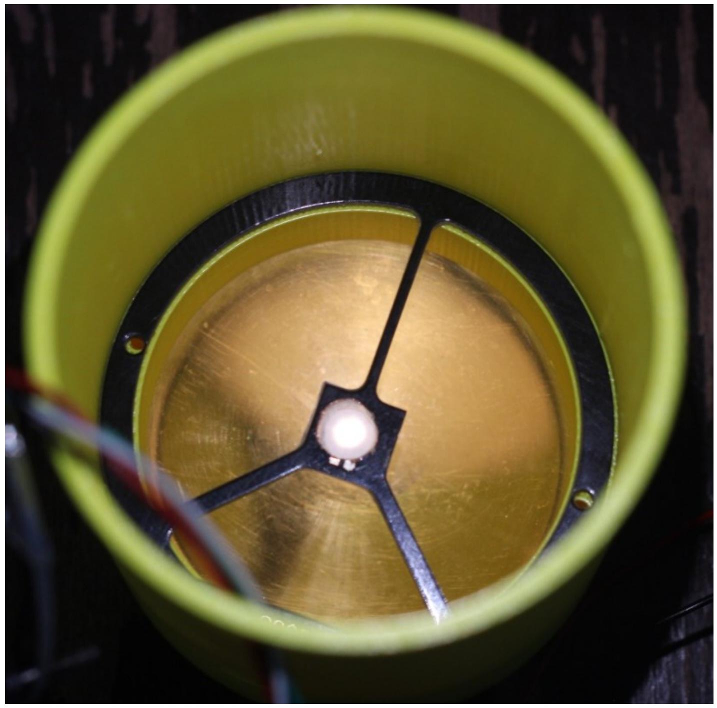

Figure 19: Mirror Focus Test

A test was conducted where the ability to focus the mirror was realized by using a sacrificial circuit board for the photodiode and drilling a hole in place of the photodiode. A small piece of opaque material such as paper was then fixed over this hole. With the laser rangefinder assembled, visible light could be shone into the laser rangefinder. This configuration allows the focused spot of the mirror to be visualized by the observer. In Figure 19 the focused spot can clearly be identified on the paper. The mirror focus could then be adjusted to minimize the spot size for maximum optical energy, taking into account the offset distance of the photodiode from the surface of the circuit board.

Chapter 4: Electrical Design

4.1. Introduction

Based on the requirements to design a laser rangefinder that would meet Size Weight and Power requirements it was known that a compact, minimal electronics design would be required. By utilizing surface mount technology, a circuit of a few components would be able to fit within a small footprint, reducing the constraint the electronics would have on the overall size of the laser rangefinder. The majority of the computation required for triggering and timing the laser pulse would be completed in a Field Programmable Gate Array, greatly reducing the number of components required in the overall design. This also provided the capability of off board processing, meaning that the only functions that would need to be completed on the laser rangefinder itself would be the pulsing and receiving functions.

4.2. Pulsing Circuit

4.2.1. Design

It was known that in order to achieve an accurate pulse, the integrity of the pulse generated would need to be maintained through consecutive pulses in addition to creating a high peak current to produce sufficient optical power for the pulse to transmit the desired distance of one kilometer. Wang Qing et al in the paper Design of High Peak Current and Narrow Pulse Driver [22] define a circuit to generate a narrow high peak current pulse through the use simple electronic components. As an FPGA is being utilized to generate the trigger pulse a portion of the circuit can be removed for simplification.

The Wang Qing design utilizes an N-Channel and P-Channel mosfet combination to provide the switching function to pulse the laser diode. Similarly a circuit proposed in the document “Drive Electronics for Pulsed Laser Diodes: Power Where it Matters” [23] which utilizes a BJT instead of mosfets and a different diode orientation. By combining each of these circuits a pulsing circuit, Figure 20, was able to be created that would generate a narrow pulse with a minimal number of components. Through simulation of it was found that the required peak current to produce sufficient optical power was not being achieved with a single mosfet, therefore a second mosfet was added in parallel with the first mosfet. These would receive the same trigger signal, switching at the same time, therefore increasing the current drain that will pass through the laser diode, in turn increasing the current optical power.

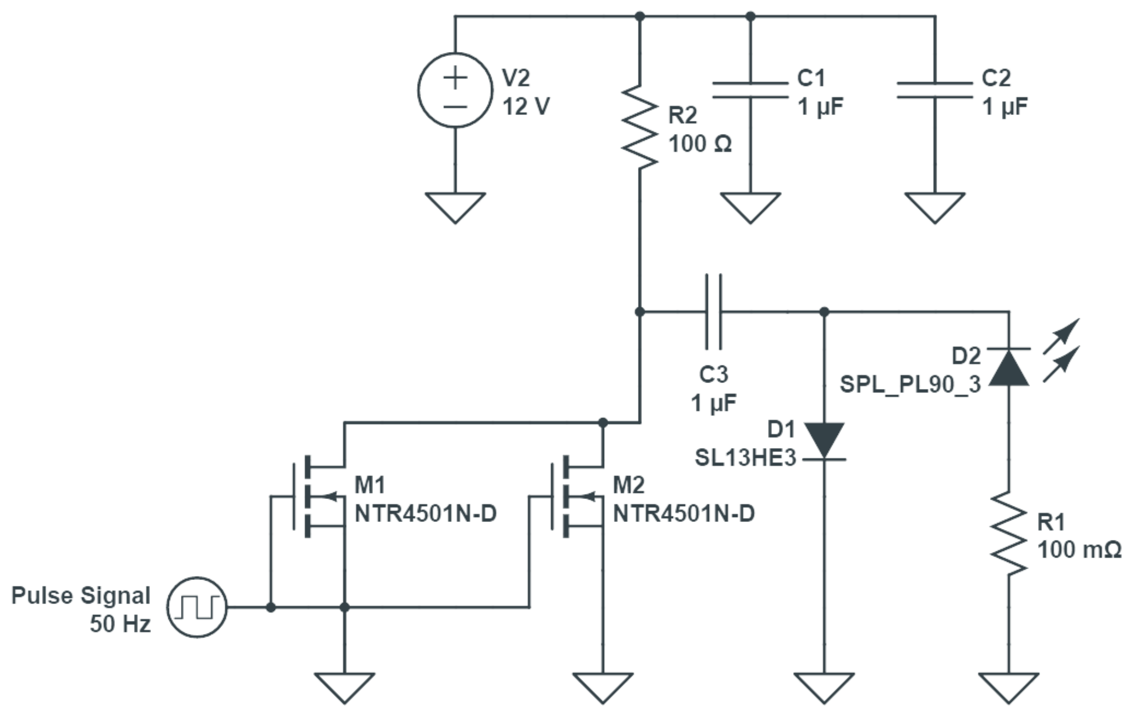

Figure 20: Pulsing circuit diagram

4.2.2. Simulation

The pulsing design was thoroughly simulated with the use of the National Instruments software Multisim [24]. This software provided the capability of using exact pSpice models of the electrical components to simulate the real-world environment. This provides the flexibility of adding components and simulating the impact of different mosfets or diodes without the need to purchase and test each component increasing certainty in the chosen components. The effect of changing a mosfet or diode can be quantified by measuring the difference in peak current of the output pulse. To measure the peak current, the voltage drop is measured across the 0.1 ohm resistor and the amperage is calculated.

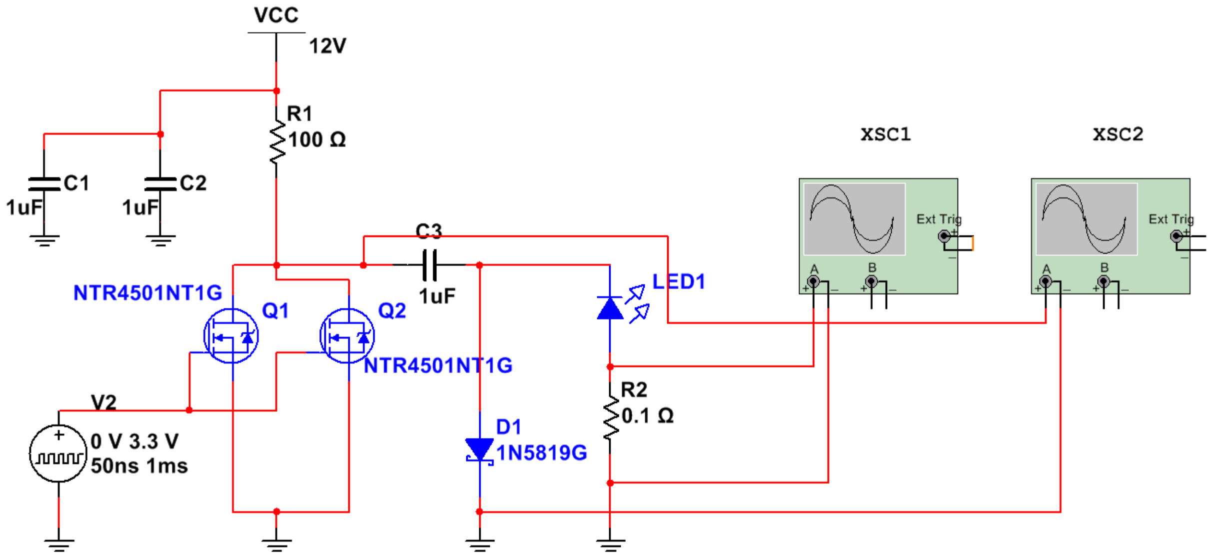

Figure 21: Multisim Circuit

In addition to the need for a high peak current output pulse, it was required that the pulsing circuit could meet the requirement for high rate of repetition. The design requirement was a minimum of 50 Hz, indicating that the circuit must create the same pulse at a minimum repetition rate of every 20 milliseconds.

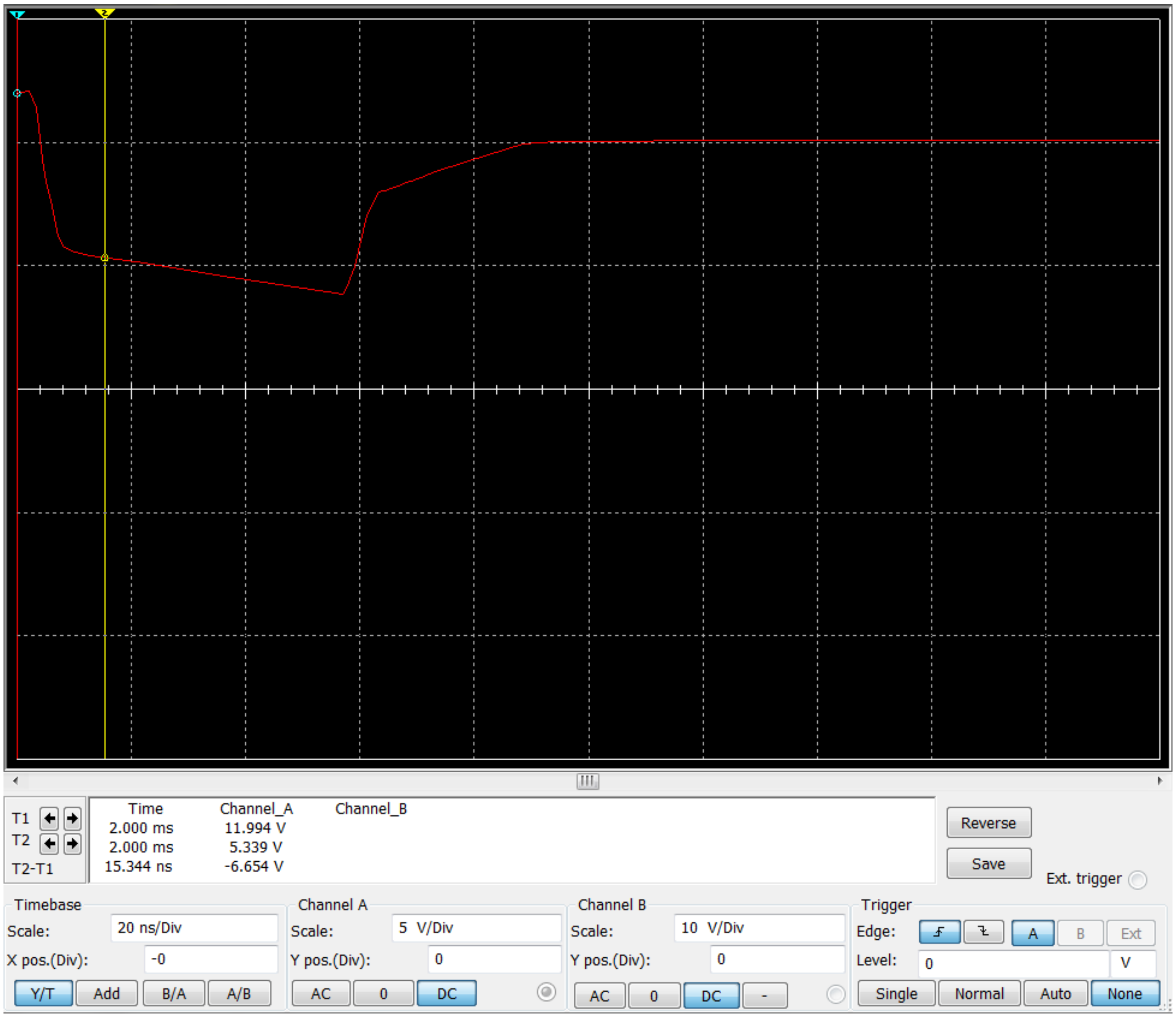

Figure 22: Multisim Oscilloscope Capacitor Discharge

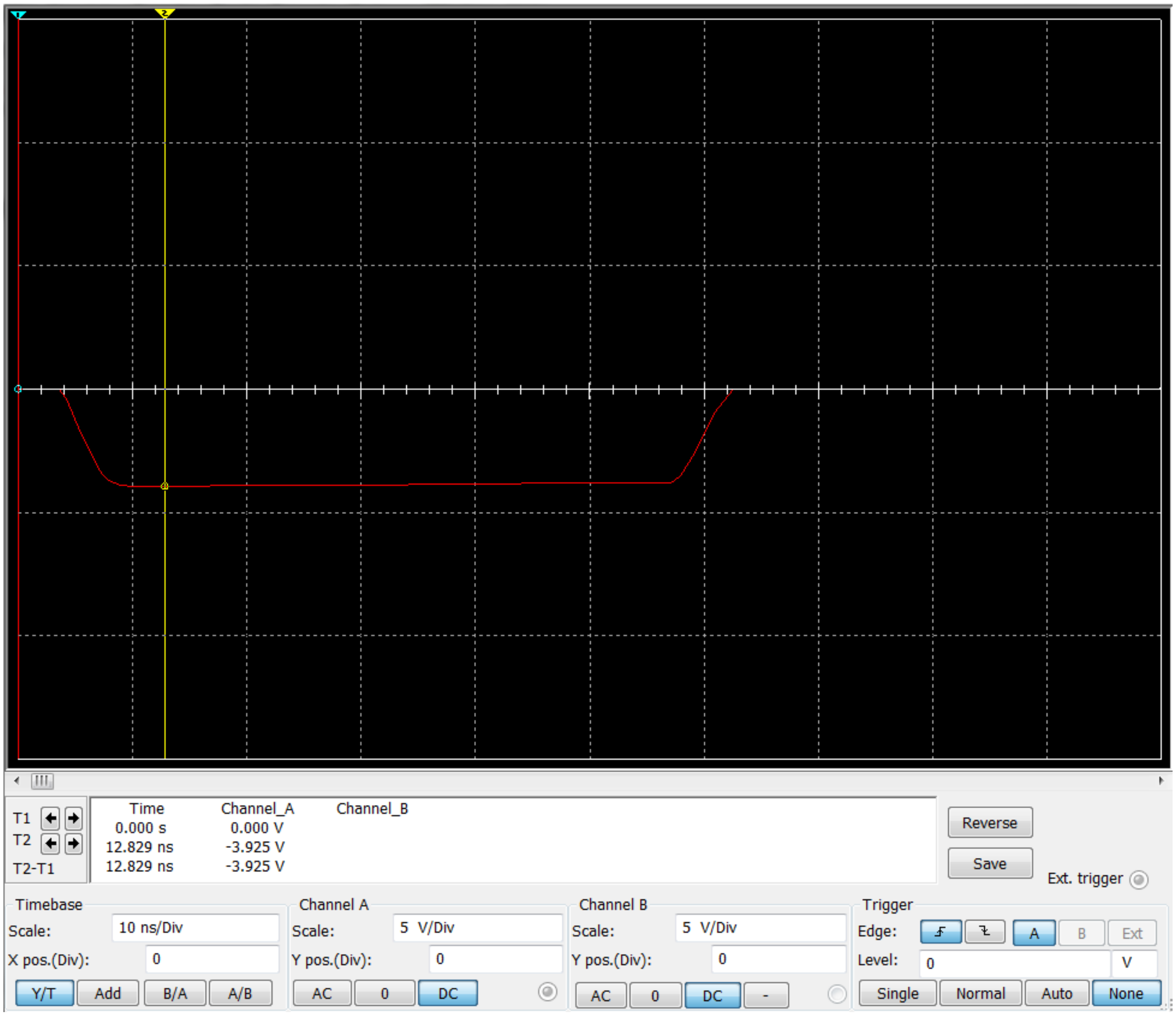

Figure 23: Multisim Oscilloscope Pulse

4.2.3. Testing

A prototype board was developed to test the ability of the circuit to create the required pulse. The purpose of this board was to identify any issues with the circuit in practical use, and therefore overall size or positioning of the components was not considered. The optimization of surface area would be completed for the final board.

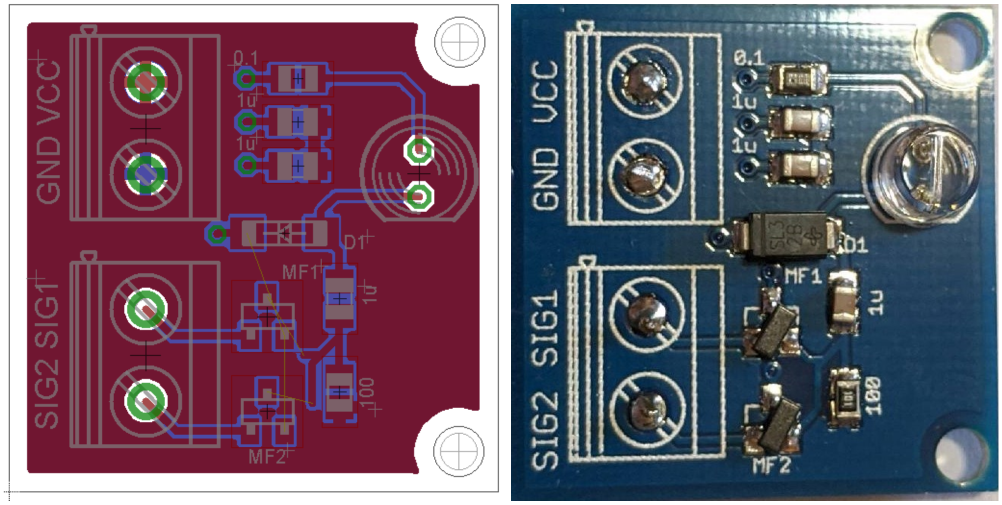

Figure 24: Prototype board design and actual

The prototype board was connected to the FPGA board to provide the pulse trigger signal and the voltage across a 0.1-ohm resistor in line with the diode was measured using an oscilloscope. Figure 25 shows the oscilloscope output of the prototype board transmission pulse across the resistor.

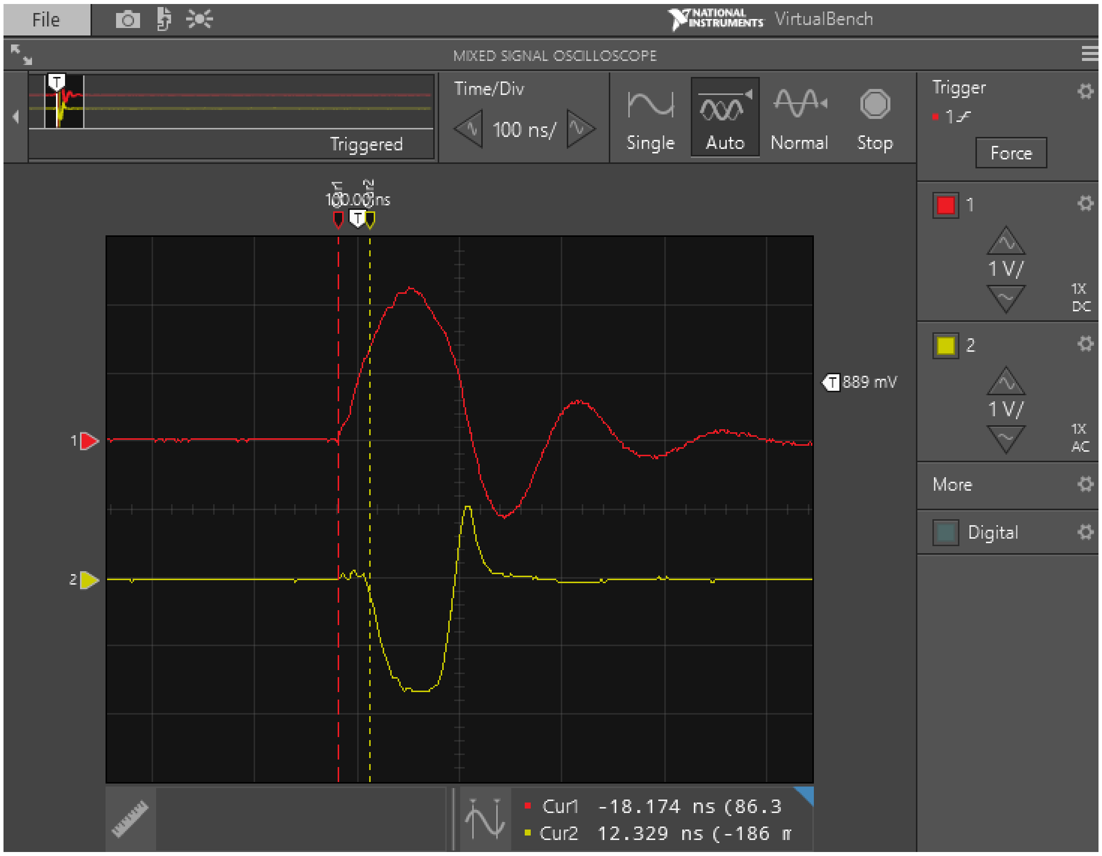

Figure 25: Transmission Pulse (trigger signal – red, pulse signal – yellow)

With successful implementation of pulsing circuit, a board revision was made taking into consideration the size and shape required to fit in the final housing design. This design stressed the importance of minimization of components and utilizing every available space on the board. The final design was able to accommodate all the required components on a double-sided board with 0.0002676 m^2 area in the optical field of view, of which most was occupied by the laser diode. The final design can be viewed in Figure 26 where the dotted lines represent the ground and power plane outlines.

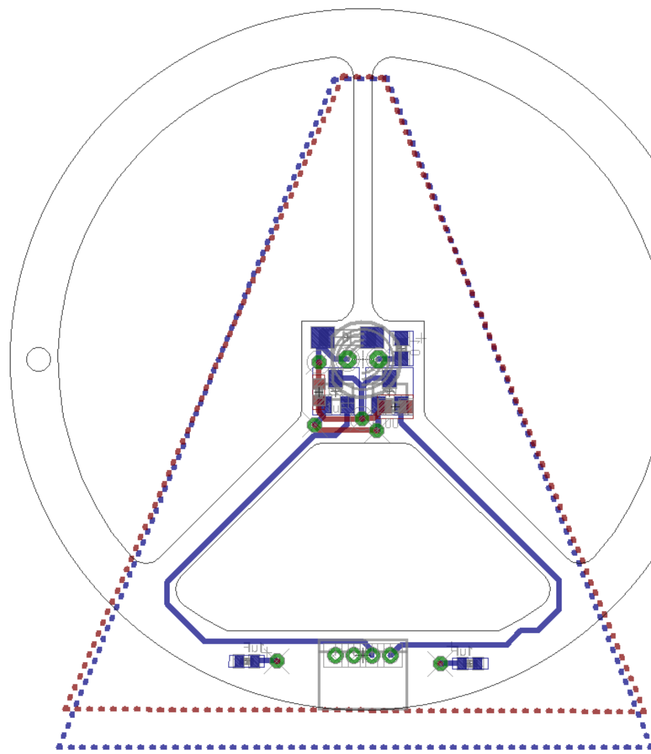

Figure 26: Final pulsing circuit board design

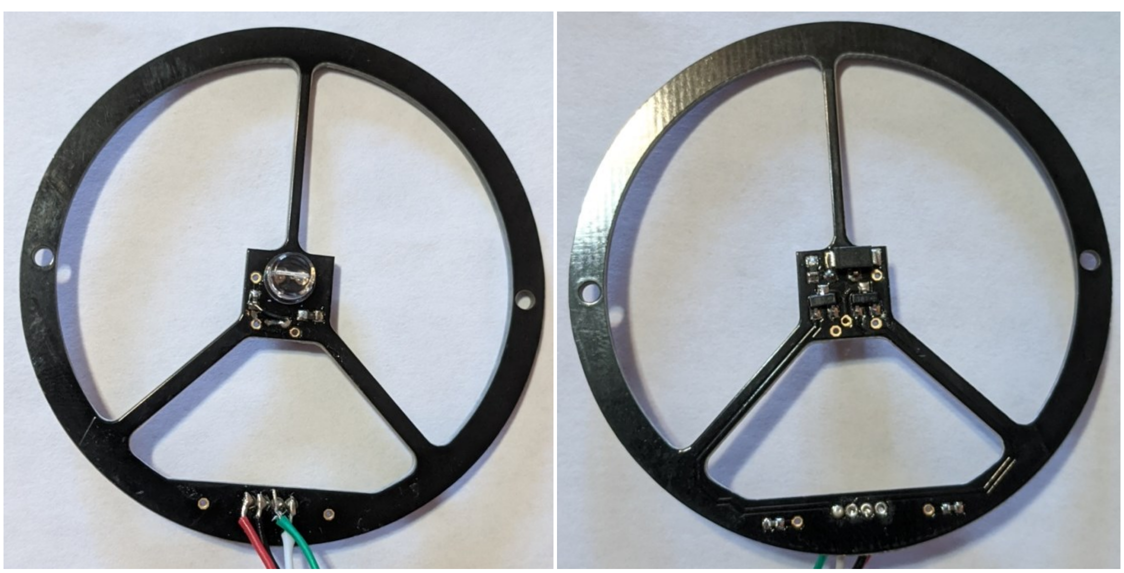

Figure 27: Final pulsing board, front (left) and back (right)

4.3 Receiving Circuit

4.3.1 Design

The receiving circuit that was used for preliminary testing of the laser rangefinder was a reverse biased photodiode, implying that the diode is grounded through a resistor, when photocurrent is received a current is generated, producing a signal that can be picked up by the FPGA, this circuit can is represented in Figure 28. The chosen photodiode was the Panasonic PNZ331CL [25], the datasheet for this photodiode provides the reverse bias circuit as a suggested method of signal capture. This photodiode was chosen as the peak wavelength of sensitivity is 900 nm and the photodiode emits a wavelength of 905nm. The physical characteristics of this photodiode also allow for ease of alignment in the designed circuit boards as it is has through-hole mounting. A comparison table of other photodiodes can be found in Table 4.

Table 4: Comparison of Photodiodes

Parameter	**Panasonic PNZ331CL**	**Vishay TEMD1040**	**Optek OPF480**	**Units**
Maximum Operating Voltage	30	60	5(typ.)	V
Photo Current	14	10	5	µA
Peak Sensitivity Wavelength	900	940	905	nm
Response Time	2	4	2	ns
Acceptance Half Angle	70	15	40	degrees
Photodetection sensitivity	0.55	0.6	N/A	A/W

Utilizing the calculations from 3.6.1 and the photocurrent characteristics of the photodiode it was predicted that the reverse diode circuit design, combined with sufficient isolation and accurate optical design, would result the laser pulse saturating the photodiode, creating adequate feedback current.

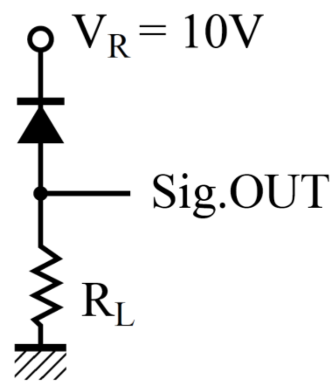

Figure 28: Reverse Bias Photodiode

With the chosen photodiode and circuit, a receiving circuit board was developed. This board used the same physical outline as the transmitting circuit board to ensure consistency in the optical path of returned light.

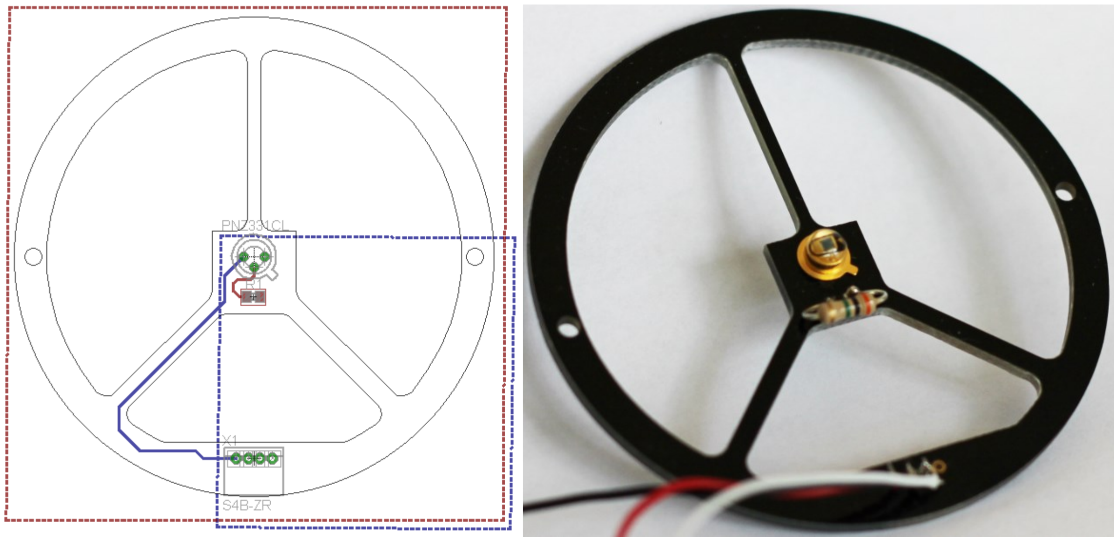

Figure 29: Receiving Circuit board with Reverse Bias Circuit, design (left) and final board (right)

4.3.2 Testing

Initial testing was completed by placing the laser diode directly face to face with the photodiode. The goal of this test was to identify a baseline that the photodiode could saturate with the laser diode. In this test the laser diode and photodiode were connected to separate power supplies. Figure 30 clearly indicates that in this arrangement, when the laser is pulsed the receiver saturates.

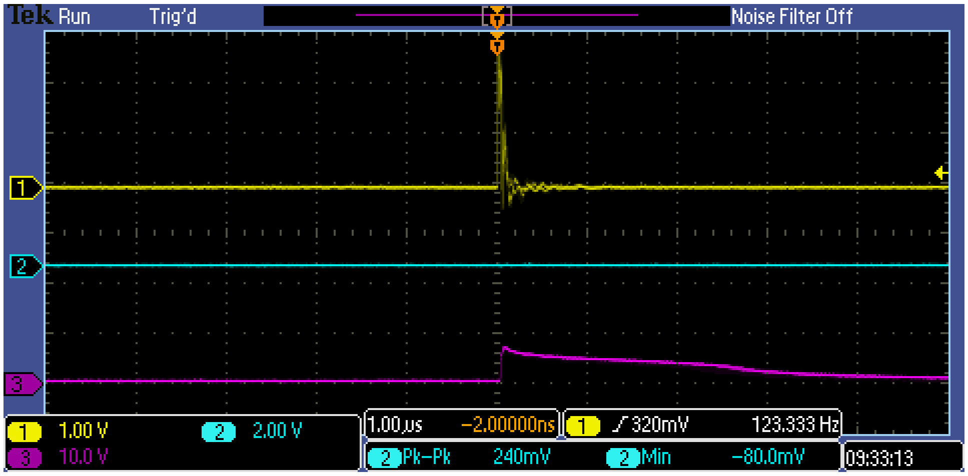

Figure 30: Face to Face Laser and Receiver (Transmission pulse - channel 1 (yellow), Ground - channel 2 (blue), Receiver - channel 3 (purple))

The next test involved assembling the laser rangefinder to see if a pulse could be captured when reflected off a surface, implying a successful optical design. In this test the pulsing circuit and receiving circuit were all connected to the FPGA to simulate the actual design environment. Similarly, as with the first test the same oscilloscope probes were connected. With this test there was a signal received by the photodiode, however there was also significant noise on the ground. This noise coincided with the pulse from the laser rangefinder. To test if the signal received was accurate, the laser diode was covered so that no light would be emitted. During this test the same results occurred, which indicates the photodiode output signal was being falsely triggered by the grounding noise from the laser pulsing circuit. It was observed that this grounding noise following the transmission pulse contained a higher frequency which was identified as is 20MHz. This corresponds to the clock of the FPGA used for timing the transmitting pulse.

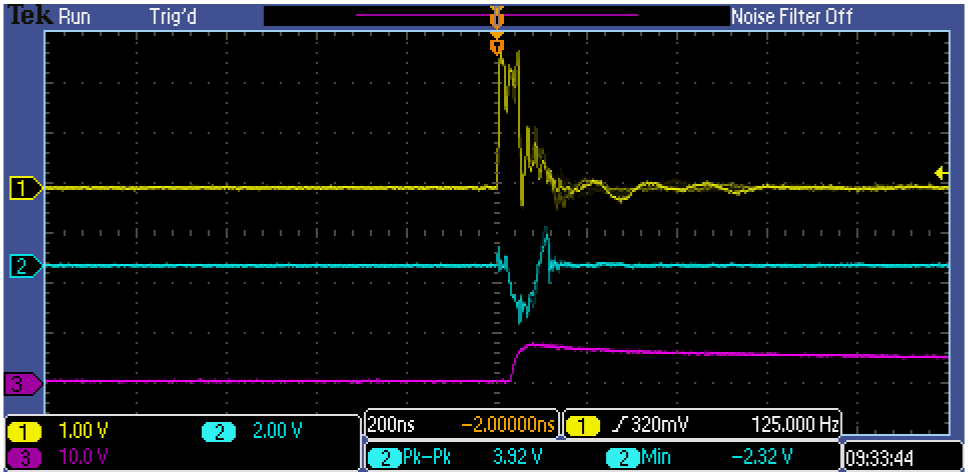

Figure 31: Transmission Pulse (Yellow) and Receiver Noise (Blue) from Oscilloscope

It was also observed that the receiver signal appeared to have a wavering component. The background voltage level measured from the receiving circuit would increase and decrease. When the time scale of the oscilloscope was increased it became apparent that there was 60 Hz interference on the receiving circuit, as shown in Figure 32. It was found that this could be removed by connecting the rangefinder housing to ground. In future development this could be incorporated directly into the housing design. The results of grounding the housing are found in Figure 33.

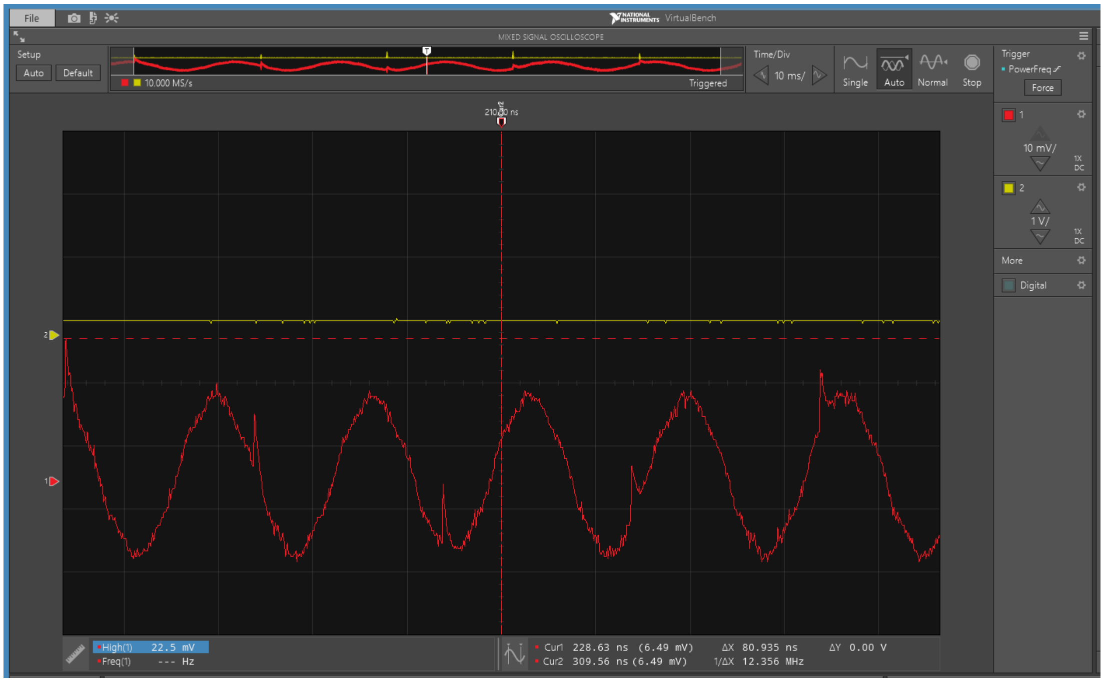

Figure 32: Receiver Signal with 60 Hz Noise

Figure 33: Receiver Signal with grounded housing

To test the second condition that the noise was generated through grounding an RF isolator was used. An RF isolator works by creating a physical separation of components within the RF isolator. Through testing it was found that this did not improve the noise. The final assumption was that the noise was simply caused by poor signal conditioning, in which a simple reverse biased photodiode was not enough to amplify the incoming infrared light and provide a high current pulse from the photodiode. To improve the signal characteristics a pre-amplifier and transimpedance amplifier was tested as described by G. Lochead [26] . Both methods involve utilizing an operational amplifier (op-amp) to either amplify the voltage, in the case of the pre-amplifier, or amplify the current, in the case of the transimpedance amplifier.

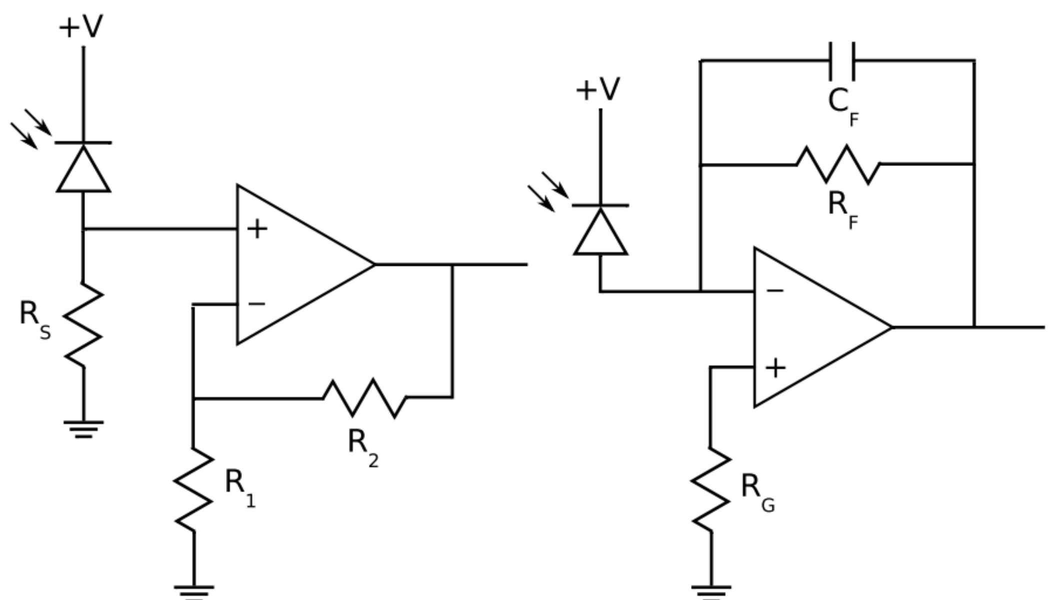

Figure 34: Pre-amplifier (left) and Transimpedance amplifier (right)

As G. Lochead [26] describes, the pre-amplifier, which utilizes a reversed biased diode, acts as a voltage amplifier as the impedance of the diode grounded resistor (Rs) makes the impedance of the photodiode negligible and the larger the resistor, the greater the voltage amplification, with R1 and R2 providing the op-amp gain. Testing utilizing this method provided amplification of the voltage measured on the oscilloscope, however it did not remove the noise.

The transimpedance amplifier was tested and similarly to the pre-amplifier a resistor controls the response, however in this case it is connected in a feedback loop from the diode to the output of the op-amp. It was found however that this method of amplification was unsuccessful.

Figure 35: Aluminum foil shielding test

With these attempts at improving the signal conditioning and grounding, it was found that the cause of the noise was likely due to RF noise. Using an RF meter on an oscilloscope the background RF noise was measured to be -80dbm away from the laser rangefinder. While the probe was within a range of 0 to 30 millimeters from the laser rangefinder the oscilloscope reading varied with a maximum of -30 dbm. With proven evidence of RF interference modifications were made to the laser rangefinder to provide shielding between the boards through the use of aluminum foil tape, Figure 35, however this did not reduce the RF impact. In order to further isolate the pulsing and receiving circuits a new laser rangefinder housing was made that would separate the boards, Figure 36. This however negates the design constraints of overall size. While testing in this configuration noise was still an issue. Further work needs to be completed in creating isolation between the devices. This could be completed through mechanical means of shielding or electrical devices such as opto-isolators. In addition, there may be the possibility of reviewing the causes of the RF noise emitted from the pulsing circuit and any options that may be available in the design of the pulsing circuit to minimize this.

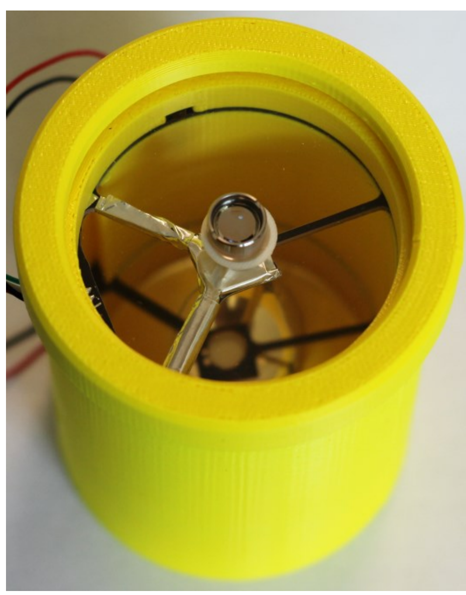

Figure 36: Extended housing isolation test

Chapter 5: Mechanical Design

5.1. Circuit Board Design

The design for the circuit board was developed based on the minimum required space to place the electrical components, as well as the minimum area required for achieving the required light to activate the photodiode. A circular design was chosen as this maximizes the receiving area with the smallest width. The diameter of the circle was chosen by adding the area required for the electrical components and support legs of the suspended center to the required area to receive light transmittance at the design distance of 1 kilometer for the design optical power as described in 3.6.1. This total area was then used to find the diameter of the circle.

Three support legs were chosen for the suspended electrical components out of structural necessity. Using a singular support leg would cause significant potential for deflection of the electrical components when the laser rangefinder was under any form of position change, such as the motion of the moving vehicle. Similarly, two support legs present the potential for rotation of the suspended board, if in a coaxial arrangement, or deflection as with the singular support leg if the legs were not aligned axially. Using three support legs provides rigidity of the centrally suspended board. The support legs were also designed to occupy the minimum amount of area while providing adequate space for electrical traces to connect the components to the external connectors. By minimizing the width of the support legs, two are able to be used to carry signal traces, while the third provides transmission through the ground and power planes to the central board.

Two mounting holes were placed on the circuit board in order to provide alignment within the laser rangefinder housing.

5.2. Housing Design

Using the circuit boards and the optical configuration as the requirements, while keeping in mind the SWaP considerations, the housing was designed to minimize the overall size, while creating ease of assembly without over complicating any components of the device to provide ease of manufacturability. The design criteria for the housing were defined by the required focal length for the transmission lens, the focal length for the mirror, spacing between the two circuit boards, and the diameter required to allow adequate light reception.

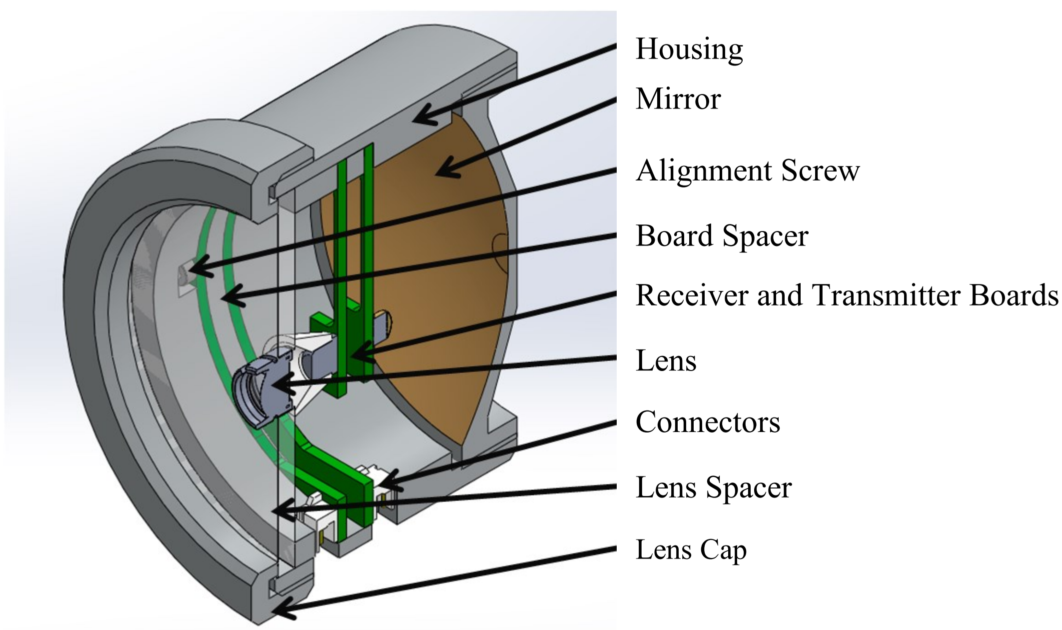

Figure 37: Complete Laser Rangefinder Diagram

A singular body comprises the housing of the laser rangefinder, this will house the circuit boards, mirror, and combination lens. As the optical design utilizes a collinear optical axis for transmitting and receiving, it was required to utilize geometric dimensioning and tolerancing to reduce the chance of error, specifically in the concentricity of components and placement of the mounting holes which align with the circuit boards.

The housing is divided into two sections, the optics and circuit section, and the mirror section. The chosen optical design for the transmission lens consists of a flat plane lens with an aspherical collimating lens mounted in the center by a fine thread, providing adjustability for focal length. Therefore, the position of the flat plane lens could be fixed relative to the circuit boards and the distance between the circuit boards and between the boards fixed with spacers. Similar to the collimating lens, the mirror required adjustment for calibration and was therefore isolated in a section of the housing which contained a fine thread, allowing for the proper focal length to be identified in testing. Additional requirements for the housing included slots which were machined through the side of the housing in order to provide access to the connectors on the circuit boards. For the prototype design a simple connector was used, however, for protection from the environment, a sealed connector would need to be specified, and adjustment to slot design would have to be made.

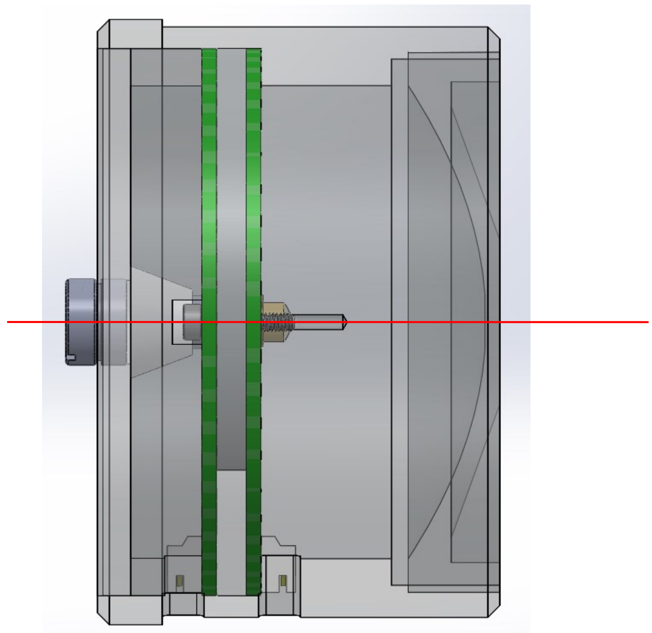

Figure 38: Laser Rangefinder Assembly Transparent View of Optical Axis

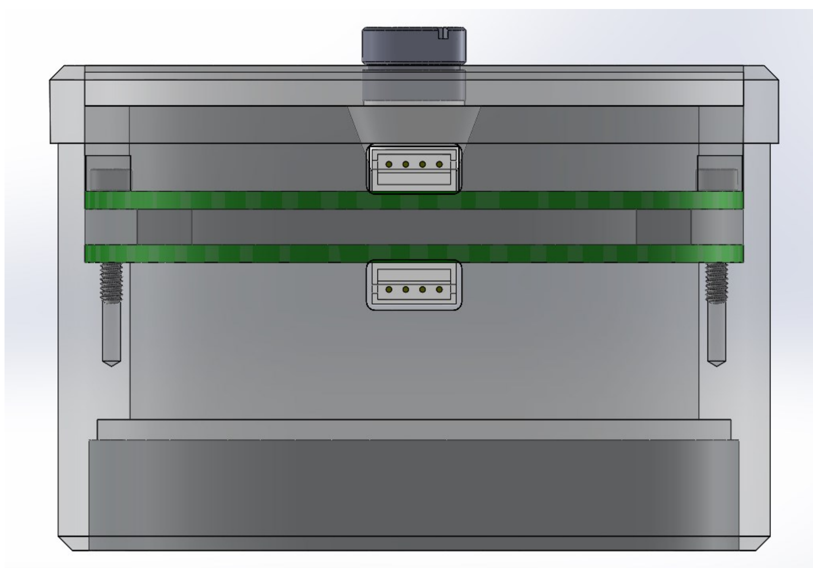

Figure 39: Laser Rangefinder Assembly Electrical Connections

In addition to the housing, three other parts were required to assemble the laser rangefinder. To seal the lens into the housing an external lens cap was designed that could thread onto the housing. For the design of the prototype the lens cap directly applies friction to the lens to hold it in place, however an O-ring face seal could be incorporated to provide protection from the environment. Two spacers had to be designed for use within the housing, one between the circuit boards, and another between the transmitting circuit board and the transmitting lens. The thickness of the spacers did not require a tight tolerance because of the adjustability built into the lens design, however, to minimize any movement of components within the interior of the housing a diameter tolerance was required.

Chapter 6: FPGA Design

6.1 Implementation

The FPGA board developed by the INSPIRUS project was used for the testing and development of the laser rangefinder. The functions of the board can be divided into two categories, timing and pulse generation and detection.

The pulse generation and detection functions could have been developed utilizing discrete electronics, however for ease of implementation and maintaining SWaP requirements these functions were also integrated into the FPGA. The capabilities of the Altera Cyclone 3 allowed the use of a phase lock loop which can multiply the internal clock speed of the FPGA. As the clock speed is directly proportional to the accuracy of distance detection.

The design of the laser range finding system was based around a state machine. The state machine can exist in a single state at a time, as specified conditions are achieved the state will change triggering different events. This state machine can be represented by a loop, where the states continuously cycle through one another. In the “done” state the program is looking for a trigger signal to begin the laser range finding process. When initiated the state changes to the “pulse” state in which a trigger is initiated to pulse the laser. When the pulse is triggered the state will change to the “timing” state in which a counter is enabled and will count at the phase locked clock speed until a received bit is identified by the receiver. With the reception of a bit the state will change to the “done” state outputting the count from the counter and await another trigger signal. A state diagram of the state flow can be found in ____.

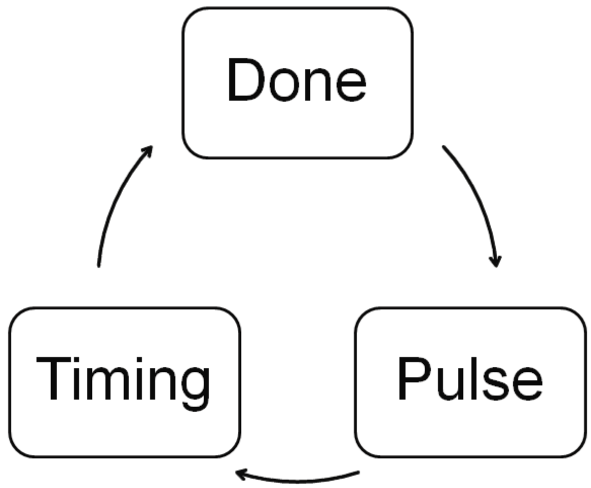

Figure 40: State diagram of FPGA Algorithm

6.1.1 Error Checking Algorithm

As there could be a potential for interference creating false positives or loss of data a signal processing algorithm could be used to ensure that the data received is accurate. An algorithm is described by Sharma, Visveswaran and Gaba [27] in which a unique sequence of bits could be transmitted rather than a single pulse. Through the use of FPGA, this sequence can be stored in a register, the incoming data can then be shifted through a register at the clock frequency and compared to the original sequence. If a match is identified it can then be assumed that the correct data has been received as a successful transmission, stopping the counter. A block diagram in Figure 41 shows the data flow through this algorithm. The utilization of signal processing will impose an inherent delay on the system as the incoming data is shifted and compared, however this can be calculated through repeated accurate tests and the delay can be removed from the timing calculation in order to provide accurate distance information.

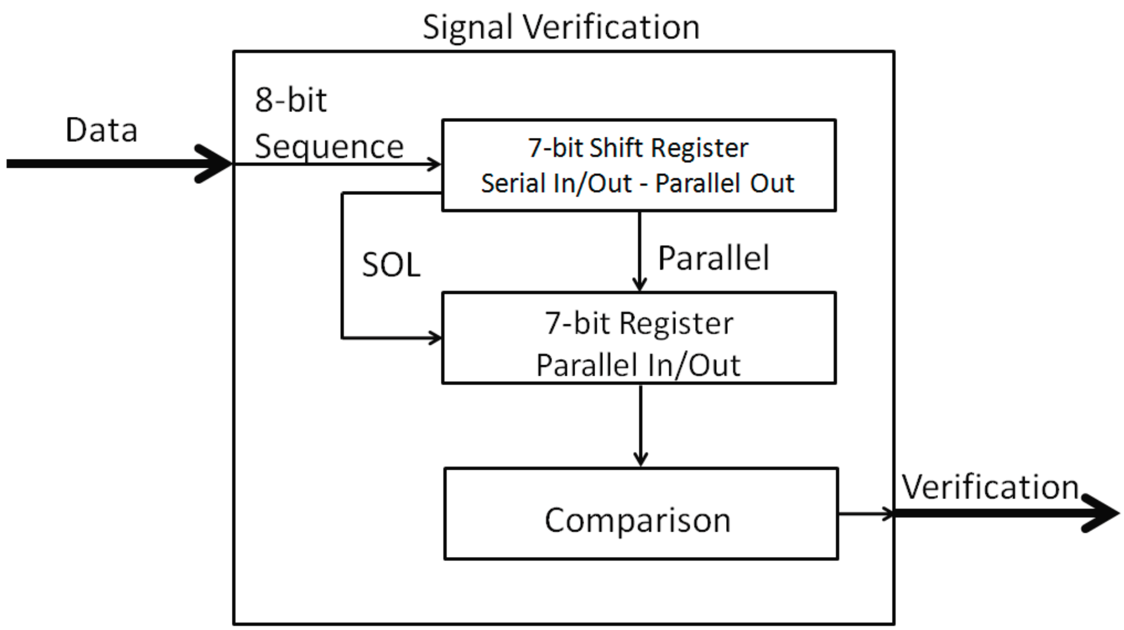

Figure 41: Error Checking Algorithm Block Diagram

A sample algorithm was created and realized on an FPGA in which the entire transmission and reception process would be simulated through the use of a serial connection with MATLAB. A code was written in MATLAB that would simulate a desired distance and 8-bit sequence representing the returned signal. This would be transferred to the FPGA, in which the distance would be represented by a clock lasting for the desired amount of time provided by MATLAB and once the time was up the 8-bit sequence was read at the clock speed into a shift register. Using the algorithm provided by Sharma et al [27], the desired 8 bit sequence is saved in a register and the incoming data is then compared to corresponding bits in each register. In order to initiate the comparison, the desired sequence must begin with a logic high (1), signaling the most significant bit of the shift register to trigger the comparison function. Once the successful comparison was identified and the distance counter stopped, the measured count would be returned to MATLAB in the form of a distance. This would then be compared to the provided distance provided and the delay of the system can be identified.

Chapter 7: Conclusions

7.1 Successes

The goal of this project was to develop a laser rangefinder that could mount on a motion platform for aerial sense and avoid applications. In order to achieve this, it would need to be small in size, lightweight, and consume minimal power.

Through the research and development process it was demonstrated that an integrated transmitting collimator and receiving lens design can be developed through a ray tracing algorithm utilizing known input and output characteristics of the optical transmitter. With minor manipulation, the same principles of this algorithm can be used to determine the output characteristics for a known lens profile and input transmitter characteristics.

Success was found in the development of a pulsing circuit that could provide the required amperage to pulse a laser diode with sufficient optical power for the design range of 1 kilometer and maintain a minimal surface area to improve light transmission past the circuit board for the single axis design. The realized circuit performed as expected based on the simulated model created using MultiSim. Utilizing this circuit with a FPGA controlling program to provide a pulse trigger the transmission portion of the project was very promising. The pulsing circuit was able to create a 30 Amp 50 nanosecond pulse at a frequency of 20 Hz with a 12-volt power supply.

In isolated testing the developed receiving circuit was able to detect the infrared signal from the transmitting pulse, validating the design theory of the receiving circuit.

However due to shielding and isolation capabilities the combination of a transmitting and receiving laser rangefinder was not possible, although each unit worked independently.

The mechanical design of the housing for the rangefinder provided a robust housing that was capable of minor adjustments to improve the ability to test the device. The housing design could easily be assembled and was lightweight.

7.2 Review of Expected Outcomes

Outcome 1: An algorithm was developed that was able to produce the lens profile for a lens capable of collimating light from a laser diode.

Outcome 2: An algorithm was developed that could produce a mirror profile able to focus ambient light to a known point.

Outcome 3: An experimental evaluation was conducted on the custom designed lens and mirror. In addition, an experimental evaluation was conducted of a commercial lens to replace custom lens.

Outcome 4: A pulsing circuit was designed and implemented meeting the design requirements.

Outcome 5: A receiving circuit was designed and implemented, however it was unable to perform as desired, not meeting design requirements.

Outcome 6: A controller was developed utilizing an FPGA that could interface with the laser rangefinder.

Outcome 7: A laser rangefinder housing was designed and manufactured and met the design requirements.

Table 5: Final Laser Rangefinder Specifications

Design Specification	Value
Diameter	63.5 mm
Weight	0.177 kg
Repetition Rate	50 Hz
Measurement Range	N/A
Accuracy	N/A
Power Supply	12V

7.3 Future Work

The theory applied to the lens design and algorithms used imply that it is possible to manufacture a single lens that will provide the required transmission and receiving optical parameters required. The limitations that were found due to the machining processes did not allow for validation of this theory. Possibilities for future testing could include submission of the design to an outside manufacturer with experience in lens development to provide more accurate test results and validation of the theory and algorithm.

The electrical components utilizing in the transmitting and receiving circuits functioned when isolated from one another, however future development is required to determine the proper amount of shielding required between the transmitting and receiving electronics to prevent interference, as the two components were successfully tested at a distance, but caused issues when in close proximity due to RF interference.

The mechanical design of the housing could benefit from improvements around weather resistance. Additional design elements that would provide increased protection from the elements such as a face seal on the lens, and O-ring in the lens cap and mirror. Additional development could be focused around robust connectors, for interfacing the laser rangefinder with the FPGA board, or an option for integration of the two systems in one unit.

Bibliography

[1] U.S. Army UAS Center of Excellence, “U.S. Army Unmanned Aircraft Systems Roadmap 2010-2035,” Fort Rucker, Alabama.

[2] Cloud Cap Technology, “TASE150 / TASE200 Compact Lightweight Daylight / IR Imaging.” Hood River, OR, 2014.

[3] Israel Aerospace Industries LTD, “MicroPOP Micro Pug-in Optronic Stabilized Payload.” Yehud, Israel, 2008.

[4] Echodyne, “EchoFlight 3D Airborne DAA Radar.” 2020.

[5] G. W. Hamilton, B. Sc, and A. L. Fowler, “The laser rangefinder,” no. September, 1966.

[6] U. S. A. E. Command and F. Monmouth, “Both systems have the disadvantage of low repetition,” no. 1, 1968.

[7] R. Society, “Mr . Isaac Newton ’ s Considerations upon Part of a Letter of Monsuur de Berce Printed in the Eight French Memoire , Concerning the Cata-Drioptrical Telescope , Pretended to be Improv ’ d and Refined by M . Cassegrain Author (s): Isaac Newton and M . Ca,” vol. 7, no. 1672, pp. 4056–4059, 2019.

[8] R. Signals and R. Establishment, “Review Laser rangefinders,” vol. 13, pp. 259–293, 1981.

[9] Bushnell, “Bushnell Legend Laser Rangefinder Owner’s Guide.” 2019.

[10] Jenoptik, “Unparalleled performance with our second-generation DLEM Laser

Rangefinders.” 2019.

[11] R. Paper, “A Review,” vol. 45, no. 4, 1995.

[12] M. The, O. Of, and P. Lasers, “Chapter 11,” 2012.

[13] J. Isoaho and A. Nummela, “Technologies and Utilization of Field Programmable Gate Arrays.”

[14] Altera, “Altera Phase-Locked Loop (Altera PLL) IP Core User Guide,” 2015.

[15] Sean Higgins, “Laser Scanning: How Does It Work, Anyway? - SPAR 3D,” 2004. [Online]. Available: https://www.spar3d.com/news/related-new-technologies/laser-scanning-how-does-it-work-anyway/. [Accessed: 14-Mar-2019].

[16] S. J. Alonso, M. Rubio, F. Martín, and G. Fernández, “COMPARING TIME-OF-FLIGHT AND PHASE-SHIFT . THE SURVEY OF THE ROYAL PANTHEON IN THE BASILICA OF SAN ISIDORO (LEÓN),” vol. XXXVIII, no. March, pp. 2–4, 2011.

[17] R. Kingslake and R. B. Johnson, *Meridional Ray Tracing*, Second. Burlington, MA: Academic Press, 2010.

[18] S. N. Kasarova, N. G. Sultanova, C. D. Ivanov, and I. D. Nikolov, “Analysis of the dispersion of optical plastic materials,” *Opt. Mater. (Amst).*, vol. 29, no. 11, pp. 1481–1490, Jul. 2007.

[19] S. M. Nejad and S. Olyaee, “Low-Noise High-Accuracy TOF Laser Range Finder,” *Am. J. Appl. Sci.*, vol. 5, no. 7, pp. 755–762, 2008.

[20] J. Wojtanowski, M. Zygmunt, M. Kaszczuk, Z. Mierczyk, and M. Muzal, “Comparison of 905 nm and 1550 nm semiconductor laser rangefinders ’ performance deterioration due to adverse,” vol. 22, no. 3, pp. 183–190, 2014.

[21] O. Loebich, “The Optical Properties of Gold,” *Gold Bull.*, vol. 5, no. 1, pp. 2–10, 1972.

[22] Q. Wang, X. Tian, G. Wu, and M. Luo, “Design of high-peak current and narrow pulse driver of laser diode,” *J. China Univ. Posts Telecommun.*, vol. 16, no. September, pp. 82–85, Sep. 2009.

[23] W. Reeb and L. C. Gmbh, “Drive Electronics for Pulsed Laser Diodes Power where it Matters.”

[24] National Instruments, “NI Circuit Design Suite.” Austin, Texas, 2012.

[25] Panasonic, *PIN Photodiode for Optical Fiber Communication Systems*. 2013.

[26] G. Lochead, “Photodiode amplifiers Pre-amplifier,” pp. 1–8.

[27] P. Sharma, G. S. Visveswaran, and S. P. Gaba, “Digital Signal Processing using Barker Code for Application in Laser Range Finder,” vol. 28, pp. 90–95, 2012.

Appendix A: Mechanical Drawings

ITEM NO.	PART NUMBER	DESCRIPTION	Default/QTY.	Manufac-tured	Sheet Number
1	LRFHousing Rev_4	Laser Rangefinder Housing	1	YES	5
2	Mirror Rev_5	Mirror	1	YES	6
3	LensSpace Rev_4	Lens Spacer	1	YES	2
4	LaserBoard Rev_2	Laser Board Assembly	1	NO	
5	CircuitBoardSpace Rev_3	Board Spacer	1	YES	4
6	0_4NA 6_24 FL M9 Mounted Asphere 64-799	Mounted Precision Molded Aspheric Lens	1	NO	
7	ReceiverBoard Rev_2	Receiver Board Assembly	1	NO	
8	Threaded Lens	Acrylic Mount For Collimating Lens	1	NO	
9	LensCap	Laser Rangefinder Housing Cap	1	YES	3
10	91290A013	Socket Head Cap Screw M2x0.4-10mm	2	NO	

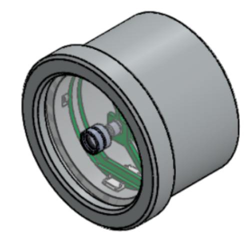

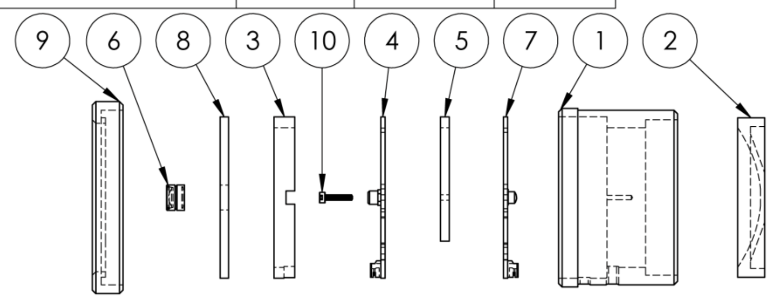

NOTE: ALL ITEMS MUST BE CONCENTRIC

UNLESS OTHERWISE SPECIFIED:
DIMENSIONS ARE IN MILLIMETERS
SURFACE FINISH: 3.2 μm
TOLERANCES:
LINEAR:
ANGULAR:

FINISH:

DEBUR AND BREAK SHARP EDGES

DO NOT SCALE DRAWING

REVISION

	NAME	SIGNATURE	DATE
DRAWN	MM		05/11/2014
CHK'D			
APPV'D			
MFG			
Q.A			

MATERIAL:

STOCK SIZE:

WEIGHT:

TITLE: Laser Rangefinder Assembly

DWG NO. LRF Rev_4 Package

A4

SCALE:1:2

SHEET 1 OF 6

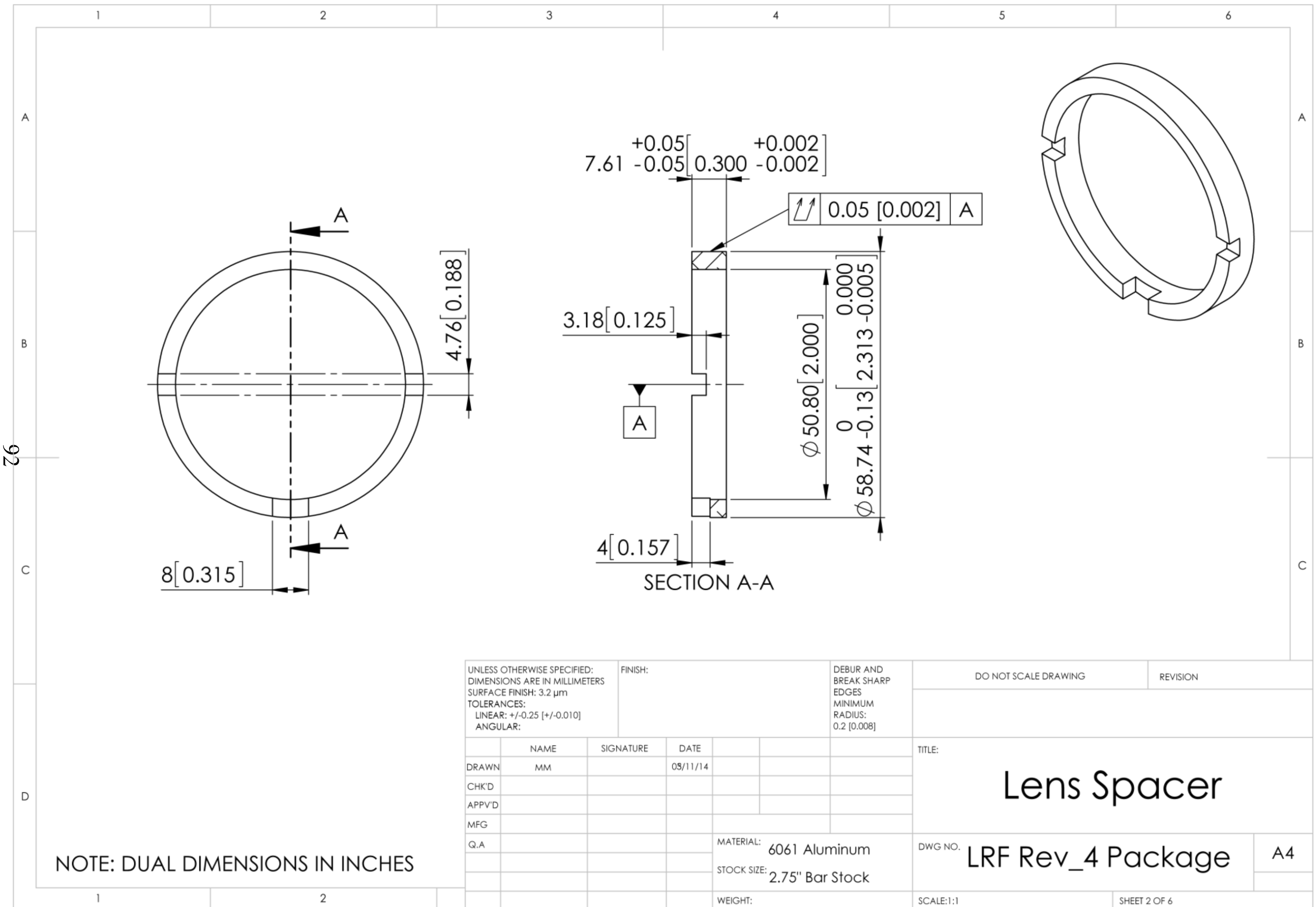
A
A
4.76[0.188]
8[0.315]
+0.05 +0.002
7.61 -0.05 [0.300 -0.002]
0.05 [0.002] A
3.18[0.125]
A
Ø 50.80[2.000]
Ø 58.74 -0.13 0 [2.313 -0.005 0.000]
4[0.157]
SECTION A-A
UNLESS OTHERWISE SPECIFIED:
DIMENSIONS ARE IN MILLIMETERS
SURFACE FINISH: 3.2 µm
TOLERANCES:
LINEAR: +/-0.25 [+/-0.010]
ANGULAR:
FINISH:
DEBUR AND BREAK SHARP EDGES MINIMUM RADIUS: 0.2 [0.008]
DO NOT SCALE DRAWING
REVISION
NAME
SIGNATURE
DATE
DRAWN
MM
03/11/14
CHK'D
APPV'D
MFG
Q.A
MATERIAL: 6061 Aluminum
STOCK SIZE: 2.75" Bar Stock
WEIGHT:
TITLE:
Lens Spacer
DWG NO. LRF Rev_4 Package
A4
SCALE:1:1
SHEET 2 OF 6
NOTE: DUAL DIMENSIONS IN INCHES

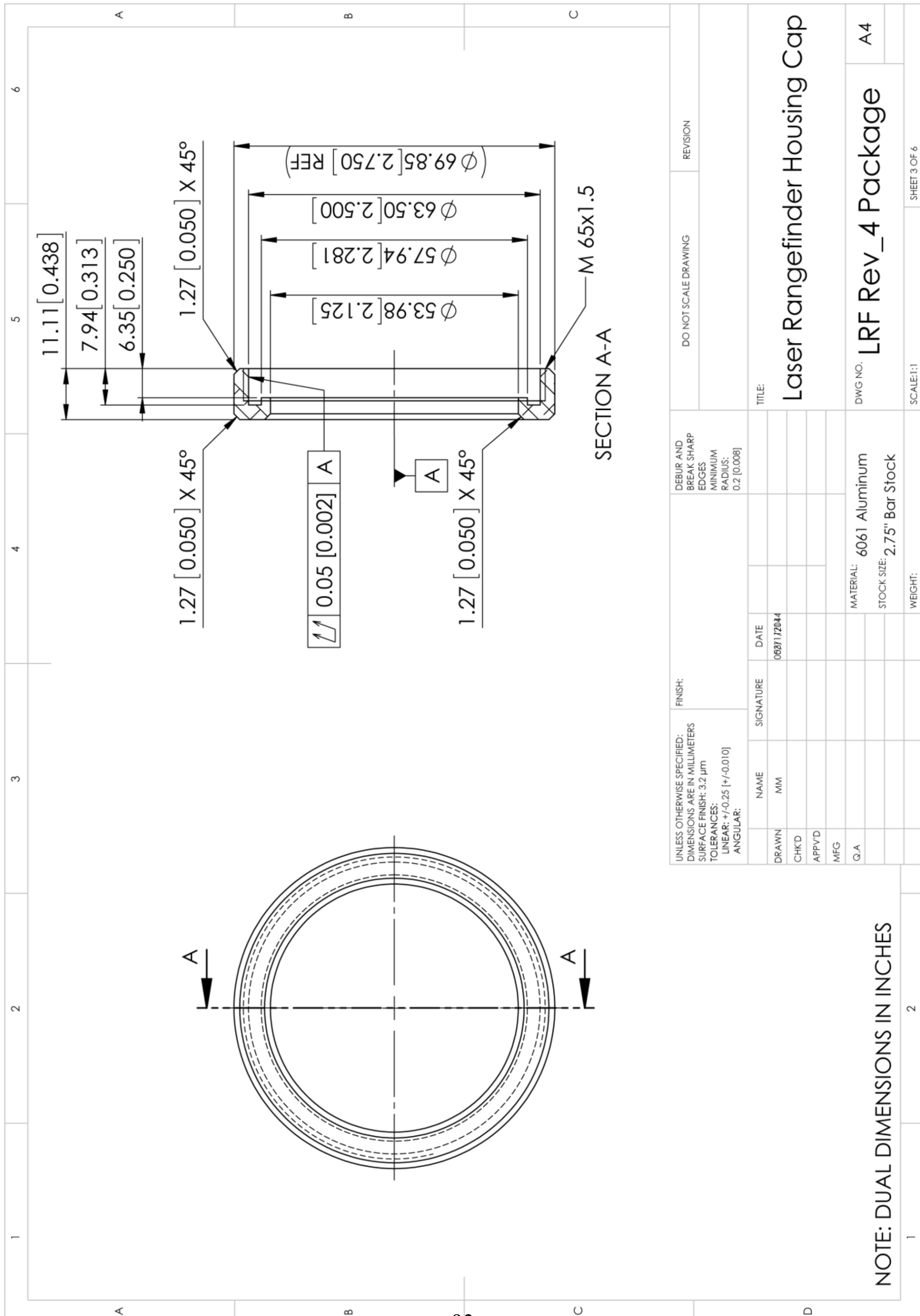
Laser Rangefinder Housing Cap
LRF Rev_4 Package
DWG NO.
TITLE:
A4
SCALE:1:1
SHEET 3 OF 6
WEIGHT:
MATERIAL: 6061 Aluminum
STOCK SIZE: 2.75" Bar Stock
DO NOT SCALE DRAWING
REVISION
DEBUR AND BREAK SHARP EDGES MINIMUM RADIUS: 0.2 [0.008]
UNLESS OTHERWISE SPECIFIED: DIMENSIONS ARE IN MILLIMETERS SURFACE FINISH: 3.2 μm TOLERANCES: LINEAR: +/-0.25 [+/-0.010] ANGULAR:
FINISH:
NAME
SIGNATURE
DATE
DRAWN
MM
CHK'D
APPV'D
MFG
Q.A
NOTE: DUAL DIMENSIONS IN INCHES
SECTION A-A
M 65x1.5
Ø 69.85 [2.750] REF
Ø 63.50 [2.500]
Ø 57.94 [2.281]
Ø 53.98 [2.125]
11.11 [0.438]
7.94 [0.313]
6.35 [0.250]
1.27 [0.050] X 45°
0.05 [0.002] A
A

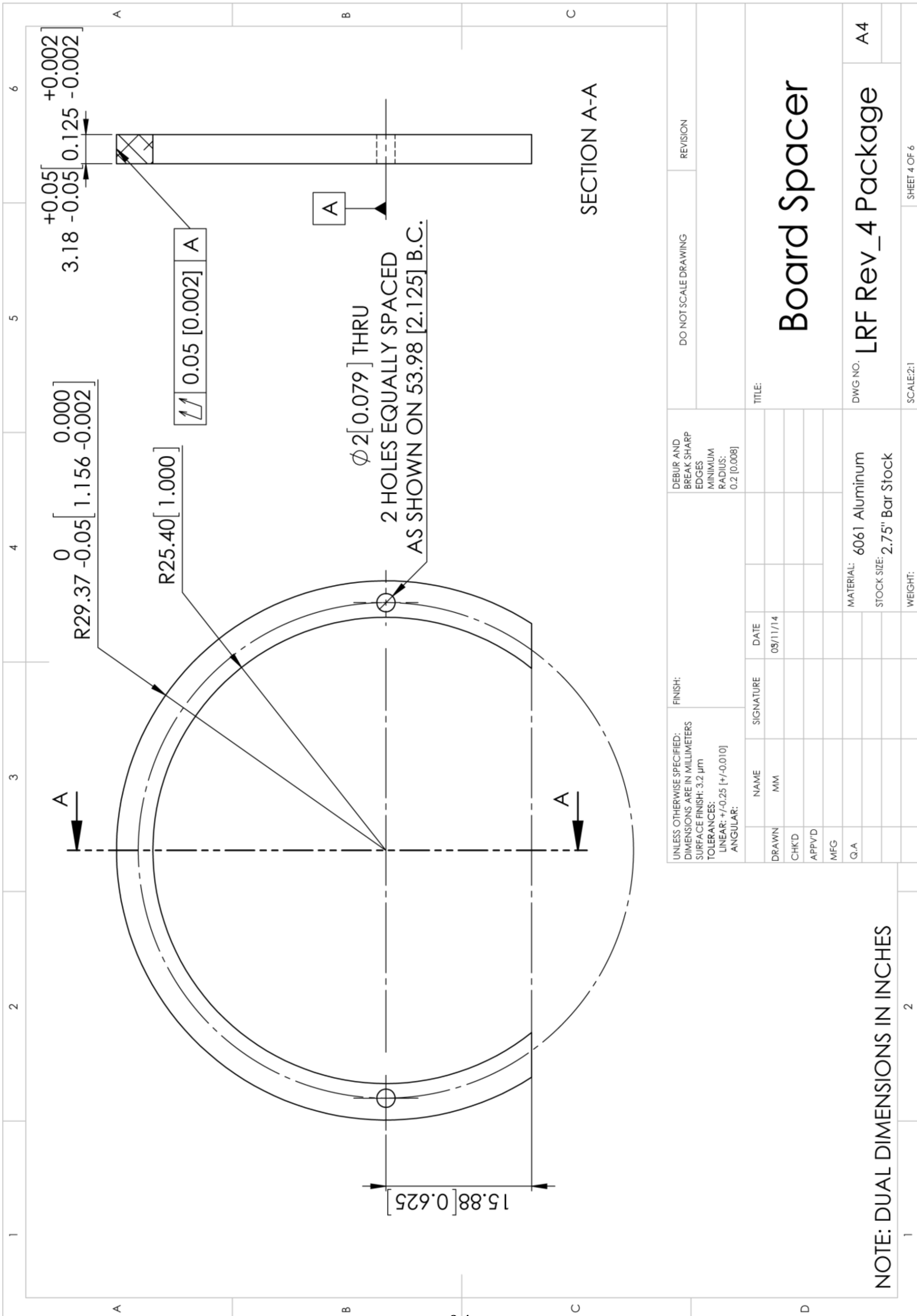

NOTE: DUAL DIMENSIONS IN INCHES
R29.37 -0.05 0 [1.156 -0.002 0.000]
R25.40 [1.000]
0.05 [0.002] A
Ø 2 [0.079] THRU
2 HOLES EQUALLY SPACED
AS SHOWN ON 53.98 [2.125] B.C.
3.18 +0.05 -0.05 [0.125 +0.002 -0.002]
A
SECTION A-A
15.88 [0.625]
UNLESS OTHERWISE SPECIFIED:
DIMENSIONS ARE IN MILLIMETERS
SURFACE FINISH: 3.2 μm
TOLERANCES:
LINEAR: +/-0.25 [+/-0.010]
ANGULAR:
FINISH:
DEBUR AND BREAK SHARP EDGES MINIMUM RADIUS: 0.2 [0.008]
DO NOT SCALE DRAWING
REVISION
NAME SIGNATURE DATE
DRAWN MM 03/11/14
CHK'D
APPV'D
MFG
Q.A
MATERIAL: 6061 Aluminum
STOCK SIZE: 2.75" Bar Stock
WEIGHT:
TITLE:
Board Spacer
DWG NO.
LRF Rev_4 Package
A4
SCALE:2:1
SHEET 4 OF 6

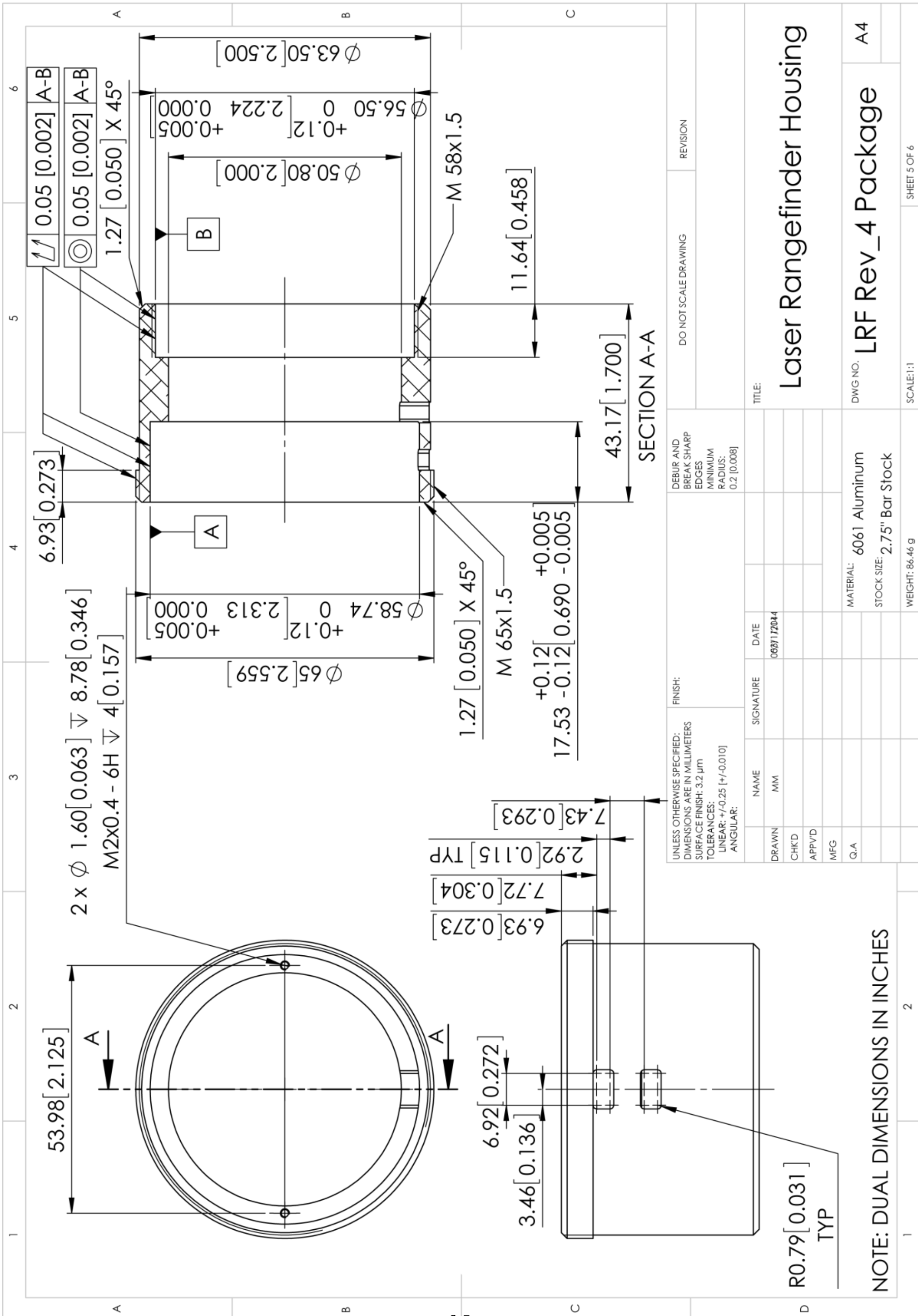

Laser Rangefinder Housing
LRF Rev_4 Package
SECTION A-A
NOTE: DUAL DIMENSIONS IN INCHES
DO NOT SCALE DRAWING
REVISION
UNLESS OTHERWISE SPECIFIED: DIMENSIONS ARE IN MILLIMETERS SURFACE FINISH: 3.2 µm TOLERANCES: LINEAR: +/-0.25 [+/-0.010] ANGULAR:
DEBUR AND BREAK SHARP EDGES MINIMUM RADIUS: 0.2 [0.008]
FINISH:
NAME SIGNATURE DATE
DRAWN MM
CHK'D
APPV'D
MFG
Q.A
MATERIAL: 6061 Aluminum
STOCK SIZE: 2.75" Bar Stock
WEIGHT: 86.46 g
DWG NO.
A4
SCALE:1:1
SHEET 5 OF 6
Ø 63.50[2.500]
Ø 56.50 +0.12 0 [2.224 +0.005 0.000]
Ø 50.80[2.000]
Ø 58.74 +0.12 0 [2.313 +0.005 0.000]
Ø 65[2.559]
M 58x1.5
M 65x1.5
11.64[0.458]
43.17[1.700]
17.53 +0.12 -0.12 [0.690 +0.005 -0.005]
6.93[0.273]
1.27 [0.050] X 45°
0.05 [0.002] A-B
2 x Ø 1.60[0.063] ↧ 8.78[0.346]
M2x0.4 - 6H ↧ 4[0.157]
53.98[2.125]
7.43[0.293]
2.92[0.115] TYP
7.72[0.304]
6.93[0.273]
6.92[0.272]
3.46[0.136]
R0.79[0.031] TYP

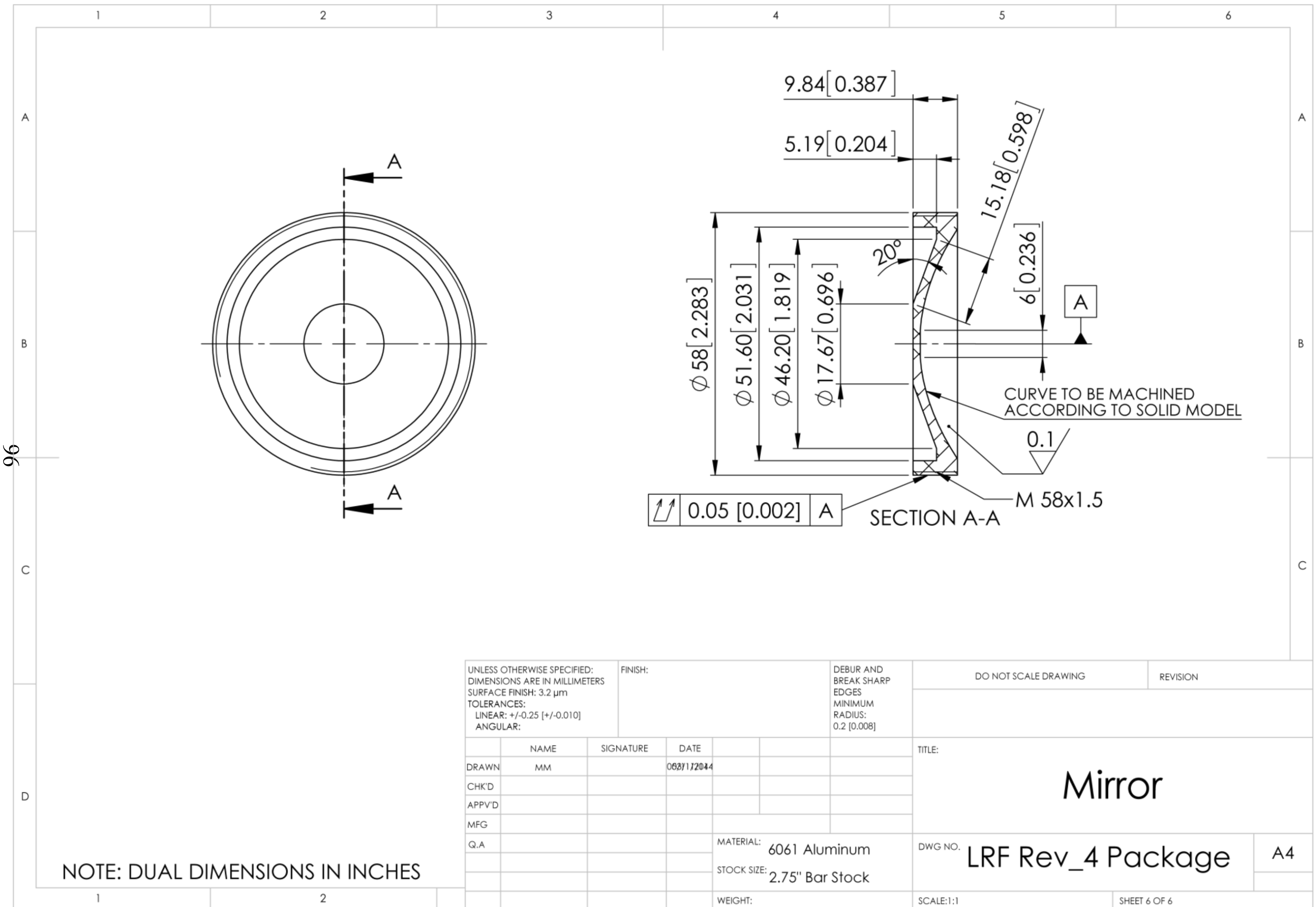

A
A
9.84[0.387]
5.19[0.204]
15.18[0.598]
20°
6[0.236]
A
Ø58[2.283]
Ø51.60[2.031]
Ø46.20[1.819]
Ø17.67[0.696]
CURVE TO BE MACHINED
ACCORDING TO SOLID MODEL
0.1
M 58x1.5
0.05 [0.002] A
SECTION A-A
NOTE: DUAL DIMENSIONS IN INCHES
UNLESS OTHERWISE SPECIFIED:
DIMENSIONS ARE IN MILLIMETERS
SURFACE FINISH: 3.2 μm
TOLERANCES:
LINEAR: +/-0.25 [+/-0.010]
ANGULAR:
FINISH:
DEBUR AND
BREAK SHARP
EDGES
MINIMUM
RADIUS:
0.2 [0.008]
DO NOT SCALE DRAWING
REVISION
NAME
SIGNATURE
DATE
DRAWN
MM
CHK'D
APPV'D
MFG
Q.A
MATERIAL: 6061 Aluminum
STOCK SIZE: 2.75" Bar Stock
WEIGHT:
TITLE:
Mirror
DWG NO. LRF Rev_4 Package
A4
SCALE:1:1
SHEET 6 OF 6